Double wall nanotubes and graphene nanoplatelets for hybrid conductive adhesives with enhanced thermal and electrical conductivity

Elena Messina,[1] Nancy Leone,[1] Antonino Foti,[1,†] Gaetano Di Marco,[1] Cristina Riccucci,[2] Gabriella Di Carlo,[2] Francesco Di Maggio,[3] Antonio Cassata,[3] Leonardo Gargano,[3] Cristiano D'Andrea,[1,‡] Barbara Fazio,[1] Onofrio Maria Maragò,[1] Benedetto Robba,[3] Cirino Vasi,[1] Gabriel Maria Ingo,[2] Pietro Giuseppe Gucciardi[1,]*

[1] *CNR – Istituto per i Processi Chimico-Fisici, Viale F. Stagno D'Alcontres 37, I-98168 Messina, Italy.*

[2] *CNR-ISMN, Area della Ricerca RM1-Montelibretti, I-00016 Monterotondo Scalo, Rome, Italy.*

[3] *Finmeccanica, Via Villagrazia 79, I-90125, Palermo, Italy*

Keywords: Graphene, Nanotubes, Liquid Phase exfoliation, Thermal interface materials, Conductive epoxy, Thermal conductivity, Electrical conductivity, Chip bonding

[†] Also at Scuola di Dottorato di Ricerca in Fisica, University of Messina, Messina, Italy.

[‡] Now at CNR-IMM MATIS, Via S. Sofia 64, 95123 Catania, Italy

[*] Corresponding author. Email: gucciardi@me.cnr.it

Abstract. Improving the electrical and thermal properties of conductive adhesives is essential for the fabrication of compact microelectronic and optoelectronic power devices. Here we report on the addition of a commercially available conductive resin with double wall carbon nanotubes- and graphene platelets- that yields simultaneously improved thermal and electrical conductivity. Using isopropanol as a common solvent for the debundling of nanotubes, exfoliation of graphene and dispersion of the carbon nanostructures in the epoxy resin, we obtain a nanostructured conducting adhesive with thermal conductivity of ~ 12 W/mK and resistivity down to 30 μΩ cm at very small loadings (1% w/w for nanotubes and 0.01% w/w for graphene). The low filler content allows one to keep almost unchanged the glass transition temperature, the viscosity and the curing parameters. Die shear measurements show that the nanostructured resins fulfil the MIL-STD-883 requirements when bonding gold-metalized SMD components, even after repeated thermal cycling. The same procedure has been validated on a high conductivity resin characterized by a higher viscosity, on which we have doubled the thermal conductivity and quadrupled the electrical conductivity. Graphene yields better performances with respect to nanotubes in terms of conductivity and filler quantity needed to improve the resin. We have finally applied the nanostructured resins to bond GaN-based high electron mobility transistors in power amplifiers circuits. We observe a decrease of the GaN peak and average temperatures of, respectively, ~ 30 °C and ~ 10 °C with respect to the pristine resin. The obtained results are important for the fabrication of advanced packaging materials in power electronic and microwave applications and fit the technological roadmap for CNTs, graphene and hybrid systems.

Introduction

Conductive adhesives (CAs) are polymeric composites containing highly conductive fillers used for chip bonding [1] and as thermal interface materials (TIMs).[2] The improvement of the electrical and thermal conductivity of CAs represents an essential technological step towards the fulfilment of present and future needs in advanced packaging systems in power electronics and microwave technology.[3] Optimization of heat dissipation at the chip-to-substrate junction and operational temperature reduction in Monolithic Microwave Integrated Circuits (MMIC) is crucially important to decrease the mean time to failure (MTTF) of the components and improve the reliability of the final device. Conventional CAs are obtained with the inclusion of micro- and nano- structured metallic fillers into epoxy or acrylic matrices.[1] Silver is preferred thanks to its excellent electrical and thermal conductivity (resistivity 1.6 μΩ-cm, thermal conductivity 470 W/mK). Silver-added CAs feature volume resistivity (ρ) down to 10^2 μΩ-cm and thermal conductivity (K_T) of some W/mK. Some higher conductivity resins, overcoming the 10 W/mK threshold can be found in the market,[4] featuring higher curing temperature, viscosity and different glass transition temperatures. In CAs the polymer resin provides the mechanical stability and the filler provides the conductivity properties. Electronic conduction occurs through the percolation network formed by the metal platelets[5] when their volume fraction exceeds a critical value (20 – 50 v/v%). Electrons flow through percolation paths formed through small contact points or by tunnelling among the flakes.[6,7] Heat conduction occurs from flake to flake through thermal contact layers. Generally no percolation is observed, due to the non-negligible contribution of the polymer matrix to the composite conductivity.[7] With the continuous shrinking of the electronic components, the thermal and electrical conductivity of the packaging represents a major bottleneck to the downscaling of the electronic circuits, due to the increasing power and current densities to be dissipated. Increasing the filler load beyond the critical filler volume is generally not a viable solution because too high fillers loadings cause the mechanical integrity of the adhesive joints to deteriorate.

Carbon-based nanostructures, among which nanotubes (CNTs) and graphene, are ideal candidates to improve the conductivity of CAs. CNTs have optimal electrical conductivity (σ ~ 10^4 – 10^5 S/m) and electron mobility (~10^5 cm^2/V s).[8,9] Double wall nanotubes (DWNT), in particular, exhibit electrical resistivity down to 10^2 μΩ-cm.[10,11] Thermal conductivity of CNTs has been reported to be in the 750 – 7000 W/mK range, i.e. 2 to 20 times better than silver.[12,13] Graphene, as well, has excellent conduction properties. Electron mobility has been reported of 2×10^5 cm^2/V s, sheet resistivity of 280 Ω per square, electrical conductivity σ ~ 10^6 S/m.[14,15] Experimental thermal conductivity values are reported in the ~ 600 – 5000 W/mK range with theoretical predictions going up to 10000 W/mK. [12,16,17] The effectiveness of carbon nanostructures has been so far tested in form of free standing films, as primary fillers in polymeric nanocomposites and as secondary fillers in silver-based conductive adhesives.

Free standing CNTs and graphene films permit to fabricate conductive ribbons[10] and thermal interfaces,[18,19] but are unsuited for large scale packaging applications. Conductive polymer embedding carbon nanostructures are indeed more versatile.[20,21] Electrically conductive composites have been reported starting from insulating polymers (σ < 10^{-11} S/m), reaching σ ~ 1 – 100 S/m[22,23,24] with some examples ramping up to 10^3 – 10^4 S/m (i.e. resistivity ~ 10^4 – 10^5 μΩ-cm).[25,26] Transmitting the thermal properties of carbon nanostructures to polymeric matrices is, conversely, still a challenge.[12,23] In early studies the CNT/graphene-polymer interface resistance[27] limited the maximum conductivities in the 0.3 – 4 W/mK range, even in presence of specifically functionalized nanostructures or of graphene/nanotubes or CNT/Ag-nanoparticles hybrids. [23,28,29,30,31] More promising demonstrations of nanocarbon-based composites for thermal management applications have been shown recently. Moon et al. [32] synthetized poly(ether-ketone)/CNT fibers with $K_T = 15$ W/mK. Yu et al. [33] synthetized a conductive epoxy resin with $K_T = 6.4$ W/mK adding graphite nanoplatelets. Li et al. [34] exploited vertically stacked multilayer graphene to achieve a nanocomposite with thermal conductivity of 16.75 W/mK, increasing to 35 W/mK at 90°C. Shtein et al.[35] produced a graphene-nanoplatelets based composite with $K_T = 12.4$ W/mK. Shahil et al. [36]

showed that the conductivity of ZnO_2-filled commercial thermal greases can be improved from 5.8 to 14 W/mK adding graphene-graphene/multilayer hybrid particles. The electrical resistivity of the nanocomposites developed so far, however, vary in the 10^5 – 10^8 μΩ-cm range, [34,35,37] indicating that polymer composites with graphitic fillers as the main conductive filler are incapable to meet the minimum requirements of next generation CAs needed in power electronics and microwave packaging applications, i.e. thermal conductivity $K_T > 10$ W/mK and resistivity $\rho < 50$ μΩ-cm.

The high aspect ratio and conductivity properties of graphitic nanofillers, however, make them a promising option as auxiliary fillers in epoxy-silver systems, where a high electrical and thermal conduction network is still granted by the metallic microstructures and the carbon nanostructures help to establish a more efficient percolation network. Electrically conductive adhesives (ECAs) with improved resistivity have already been developed by the addition of graphitic nanofillers decorated with silver nanoparticles (see ref.[38] for a review). Oh et al.[39] synthetized an ECA with resistivity of 40 – 50 μΩ-cm and an Ag-paste with resistivity of 18 μΩ-cm using acid-treated and metal-plated (nickel, silver) CNTs. In a further work[40] a silver-filled ECA with resistivity of 4 μΩ-cm was demonstrated adding a small amount (1.5% w/w) of MWNTs decorated with Ag nanoparticles (NPs). For what concerns graphene, Liu et al.[41] were able to bring the resistivity of the ECA from 700 μΩ-cm down to 43 μΩ-cm adding only 0.05% w/w of Ag-decorated graphene platelets (GNPs). More recently Amoli et al.[42] showed a reduction of the resistivity of an ECA from 550 μΩ-cm to 46 μΩ-cm adding graphene decorated with silver NPs (1% w/w) and increasing the curing temperature form 150 to 220 °C. No information on the thermal conductivity of the composites is given in these works. To the best of our knowledge, the only example of metal-filled conductive adhesive with improved thermal conductivity thanks to graphene addition has been reported by Goyal at al.[43] Starting from a conductive silver-filled epoxy ($K_T \sim 1.7$ W/mK), the authors reached a thermal conductivity of 10 W/mK adding 5% v/v of few-layers graphene dispersed in water/surfactant solutions. The reported resistivity was, however, very large (~ 10^4 μΩ-cm) and did not change with the addition of graphene.

These results leave the promise of a simultaneous improvement of both electrical and thermal conductivity thanks to graphitic nanofillers still unmet. For large scale applications, moreover, advanced CAs must also feature a balanced viscosity ~ 10^3 cP, to ensure small spotting and allow for automated applications; a low curing temperature, < 150 °C, preventing components failure during the melt of the solder alloy is also a must; high die shear strength, even after repeated thermal cycling, is necessary to ensure chip bonding during applications in severe temperature conditions. In this framework, the possibility to improve the conductivity of adhesives already used in the production lines and fulfilling the above cited requirements is highly desirable.

In this work we have modified a commercially available silver-filled conductive adhesive ($K_T = 2.5$ W/mK, $\rho \leq 400$ μΩ-cm, viscosity 2000 – 3000 cP) with small quantities of DWNTs (1% w/w) and graphene nanoplatelets (0.01% w/w) to obtain a nanocomposite with simultaneously improved electrical resistivity (best value $\rho = 30$ μΩ-cm) and thermal conductivity (best value $K_T = 11.8$ W/mK). The use of isopropyl alcohol as a common solvent for the separation of the carbon nanostructures and the dispersion in the epoxy resin is a key point that allows us to obtain CAs with improved conductivity with pure graphitic nanofillers, without the requirement of any additional metal decoration. Thanks to the low filler content the curing parameter, the viscosity and the mechanical properties are not substantially altered, satisfying the MIL-STD-883 standard. We have further tailored the preparation methodology to a more viscous, higher conductivity resin ($K_T = 11.9$ W/mK, $\rho \leq 80$ μΩ-cm, viscosity ~ 6000 cP), bringing the resistivity down to a minimum of 9 μΩ-cm, and the thermal conductivity up to 19.6 W/mK. We finally used nanostructured resins to bond GaN power transistors and show a decrease of the average junction temperature of the RF power amplifier by 10 °C.

Materials and Methods

Materials

Isopropanol, and Tetrahydrofuran have been purchased from Aldrich and used as received. DWNTs (purity of 99,5%), DWNTs functionalized with COOH and NH_2 terminal groups (purity 95%), and MWNTs (purity > 95%) are purchased from NanoLab. Nominal diameters and lengths of the DWNTs are 1 – 4 nm and 1 – 5 µm, respectively. MWNTs have diameters and lengths of 15 – 30 nm and 5 – 20 µm, respectively. Natural flake graphite are purchased from Sigma-Aldrich. We work with a commercial two-components silver-filled epoxy resin, largely employed for chip bonding in electronic and microwave power devices. The resin is based on a DOW epoxy novolac and on a modified amine, respectively, for the epoxy component (part A) and hardener (part B). The system contains ~ 78% w/w silver in the form of platelets with size in the 1 to 15µm range and contains smaller silver nanoparticles with dimensions between 500nm and 1 µm (see Figure S1 in Supporting Information). According to the producer's specifications, the resin has thermal conductivity $K_T = 2.5\ \mathrm{W/mK}$, resistivity $\rho \leq 400$ µΩ-cm, viscosity ~ 2200 – 3200 cps, glass transition temperature $T_g \geq 80\ \mathrm{°C}$, curing temperature/time parameters ranging from 80 °C / 3h to 150 °C / 5 min.

Nanotubes dispersion

Nanotubes tend to aggregate into ropes or bundles causing poor dispersion in polymer matrix if used as purchased. Ultrasonication followed by ultracentrifugation allows one to debundle the nanotubes in watery solutions[44] and in solvents suitable for dispersion in polymers.[45] In this work we have dispersed different types of carbon nanotubes (double-wall, DWNT, either pure or functionalized with –COOH and –NH_2 groups, multi-wall, MWNT) in Isopropyl alcohol (IPA) through horn ultrasonication (Branson Sonifier 250). CNTs quantities ranging from 33 µg/mL to 13 mg/mL (corresponding to weight fractions of 0.01% to 4% with respect to the total resin) have been sonified for 30 minutes in IPA with the help of an ice bath to avoid overheating. The solutions thus

obtained are immediately mixed with the resin, in order to prevent flocculation and re-aggregation that, for DWNT at concentrations higher than 0.5%, is visually observed typically after 30 min.

Liquid phase exfoliation of graphene platelets

Graphene nanoplatelets are prepared by liquid phase exfoliation (LPE) [46] of Highly Ordered Pyrolitic Graphite (HOPG) via sonication in IPA[47] using an ultrasonic bath (Soltec SONICA 1200M, 160 W peak power) for 2 hours. The obtained solutions are stable up to a volume concentration of 0.5 mg/mL. As for CNTs, the graphene solutions are used immediately.

Synthesis of the nanocomposite

To embed the carbon nanostructures in the resins we use the "*in situ polymerization*" approach and tailor to silver-filled adhesives a procedure developed for mechanical properties enhancement with graphene (see Figure 1).[48] The strategy aims at maximizing the dispersion of the nanostructures at the molecular level into the one component of the resin using a common solvent to disperse the CNTs (Figure 1a), exfoliate the graphene (Figure 1b) and dissolve the epoxy component of the resin (Figure 1c). The nanostructures are thus added to the part A. After solvent removal (Figure 1d), we include the hardener (part B) using automated mechanical shear mixing procedures (Figure 1e) to produce a homogeneous nanocomposite (10g of resin are produced after each process). As for the solvent, we have evaluated tetra-hydrofuran (THF), water and IPA. IPA has been chosen since it is also an effective solvent for the part A of the resin. It is volatile and has a low boiling point (82 °C), a definite advantage for solvent removal during the composite preparation. IPA is capable to debundle CNTs and exfoliate grafene. [47] Although its dispersion properties are limited with respect to surfactants, IPA represents a reasonable trade off between the need of a common solvent and the more effective surfactant-assisted procedures for CNTs debundling[44] and graphene exfoliation,[46] that require the use of water as solvent.

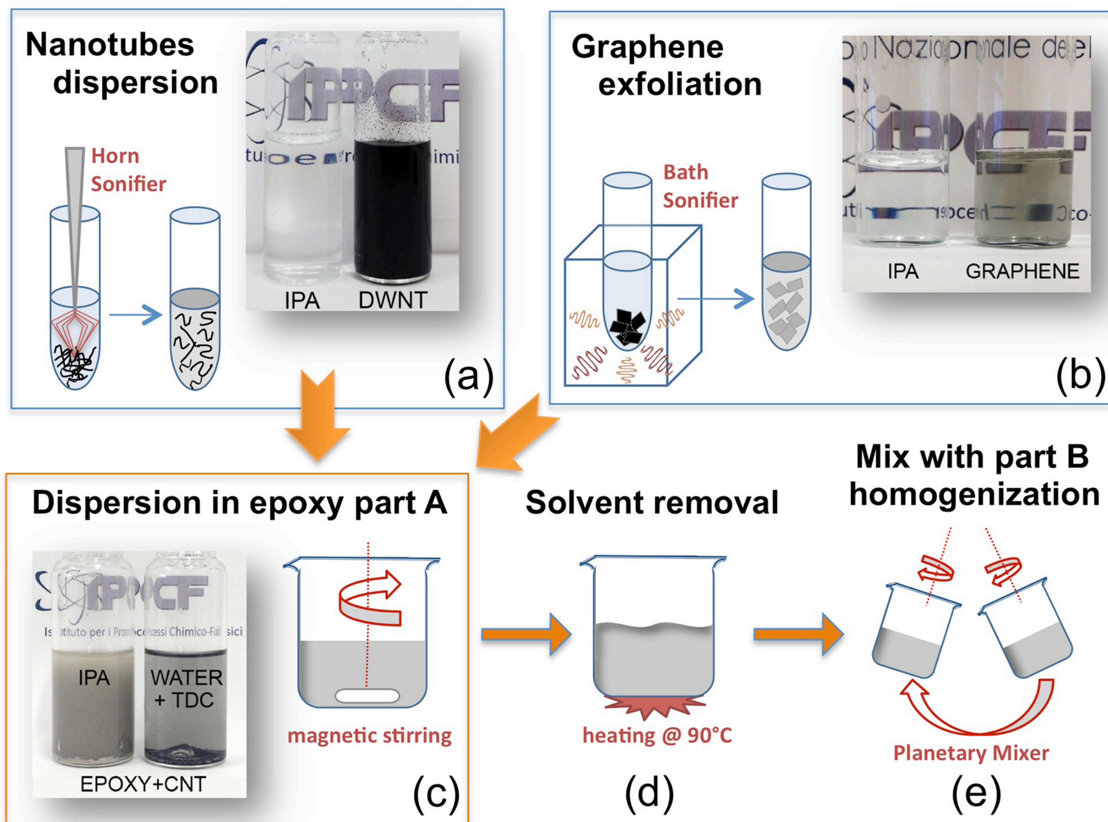

Figure 1: Schematic of the preparation of nanotubes- and graphene- silver-filled epoxy resin composites. (a) Dispersion of carbon nanotubes is accomplished through horn sonication of CNT powders in IPA. The picture shows a CNT solution (3.3 mg/mL) just after sonication. (b) Graphene exfoliation in IPA is carried out through bath sonication of graphite. The picture shows a stable graphene solution (250 μg/mL) after 1 month from the preparation. (c, left hand side vial in the picture) The CNTs-IPA solutions easily dissolve the part A of the resin which, instead, precipitates when a solution of CNT dispersed in water + TDC is added (right hand side vial in the picture). (d) The nanostructures solutions added to the part A are subject to magnetic stirring and heating at 90 °C for solvent evaporation (d). The part B of the resin (e) is added to the part A and homogenised through shear mixing in a planetary mixer.

The insolubility of our resin in water is, in fact, the main obstacle preventing us from using these latter methodologies.[43] In Figure 1c we show, in fact, the different effect of the two solvents, comparing a sample (left hand side vial) of part A mixed with CNTs dispersed in IPA, with one (right hand side vial) of part A mixed to CNTs dispersed in water + taurodeoxycholate following standard procedures.[44] In the latter case we observe the precipitation of the part A and the re-

aggregation of the nanotubes on the surface of the resin. THF has been excluded because of the limited improvement or even worsening of the conductivity of the resin (vide *infra*). To disperse the nanostructures into the epoxy matrix, we add the solutions to the part A (5g) in a glass Becker where they undergo magnetic stirring for 30 min (Figure 1c). Subsequently, the mixture is heated at 90 °C for ~ 30 min for solvent removal (Figure 1d). When IPA is evaporated, the part B (5g) is added and homogenized with the part A-nanocomposite mixture by using a planetary mixer (ARE-250, Thinky, Japan, Figure 1e). We work for 10 min at 2000rpm in mixing mode and for further 10 min at 2000 rpm in defoaming mode, in order to remove air bubbles formed during the mixing stage. Curing is accomplished according to the epoxy specifications, either in an oven or in a hot plate.

Optical characterization.

UV-VIS spectroscopy has been used to estimate the concentration in our GNP solutions. This is done by applying Lambert-Beer law to the measured absorbance at 660nm. [46,47] Measurements have been carried out with a Perkin Elmer Lamda 25. Cuvettes l = 1cm large are used. The Lambert-Beer law is used to estimate the concentration, c, of graphene in the solution based on the relation $A = \alpha c l$ among the absorbance, A, the molar extinction coefficient, α, and the optical path length, l.

Raman spectra are collected at room temperature with a Jobin-Yvon HR800 micro-spectrometer operating with a 514.5nm laser source. Light is focused on a ~ 600nm diameter by a 100X NA 0.95 objective. Laser powers < 1 mW are used to prevent overheating and damaging. A drop of solution was cast on a silicon oxide substrate and analysed after solvent evaporation.

Thermal conductivity

Thermal conductivity is measured using a Hot Disk Thermal Analyser TPS500 (Hot Disk AB, Uppsala/Sweden) based on a transient technique. The sensor (3 mm diameter) supplies a heat-

pulse of 0.03 W for 20 s to the samples and the associated change in temperature is recorded. Measurement are performed at room temperature. Disk-shaped samples (20 mm diameter,10 mm ness) are required, prepared using a teflon mold.

Electrical conductivity

Electrical resistance is measured with multimeter (HP3478A) in a 4-wire configuration. Measurements are carried out on thin films (60 μm thickness, 4 mm width, 7 cm length) produced with the doctor blade (or tape casting) technique: two parallel strips of tape are attached on a glass slide and the nanostructured resin is cast in the central canal with a putty knife. In order to calculate the information on the resistivity of the material, the thickness of the sample film is measured locally with a stylus profilometer (Dektak XT, Bruker) and with a micrometric screw for averaging on larger areas.

Morphological analysis

The morphology of the samples is investigated by using a high brilliance LEO 1530 (FE-SEM) scanning electron microscope.

Viscosity analysis

Viscosity measurements are carried out with a Brooksfield DV2T viscometer, equipped with a CPA-52Z conic spindler.

Thermodynamic analysis

We have used a Mettler Toledo DSC1 differential scanning calorimeter. Ca. 15 mg of resin have been analyzed for determining the curing profiles. The temperature ramp is extended from 25 ° C to 300 ° C and a temperature increase of 10 ° C per minute. For the isothermal measurements we have used ca. 17 mg of sample, sampling the heat flow at steps of 30s for the curing at 135°C

and steps of 120s for the curing at 90°C. For the determination of the T_g, ca. 25 mg of cured resin have been subject to a temperature ramp from ambient to 150 °C, increasing at a rate of 10 °C per min. Mechanical properties of cold-drawn films (loss and dynamical storage modulus, E'' and E' respectively) were measured in the 25–180 °C temperature range by a dynamical mechanical thermal analyzer from Triton Technology (TTDMA). Dynamical experiments have been carried out using a bending geometry in a single cantilever configuration. The temperature scan rate was fixed at 2 °C/min with an accuracy of 0.1 °C and the frequencies were set to 1 and 10 Hz for all samples.

Thermal imaging

Infrared thermography is capable to map temperature distribution of an electronic device in a non destructive, contactless way. We have employed a thermal imaging infrared camera (FLIR MOD SC325 – 60 Hz) to acquire quantitative thermal maps of GaN power transistors and highlight the temperature distribution when the components are bonded with the different resins.

Die shear analysis

Die shear measurements have been performed to measure the maximum lateral force that can be applied to an SMD component bonded to a gold surface before detachment. Die shear measurements have been carried out with a fully automated DAGE series 4000 Multi-Function Bondtester. Chip bonding is done manually following well assessed internal standard procedures for devices production.

RESULTS

Morphology of the CNT-added composite

Figure 2a shows the Scanning Electron Microscopy (SEM) picture of a nanocomposite sample obtained with the addition of DWNTs (1% w/w). The nanotubes show up as a network of 1D structures, well dispersed in the epoxy matrix.

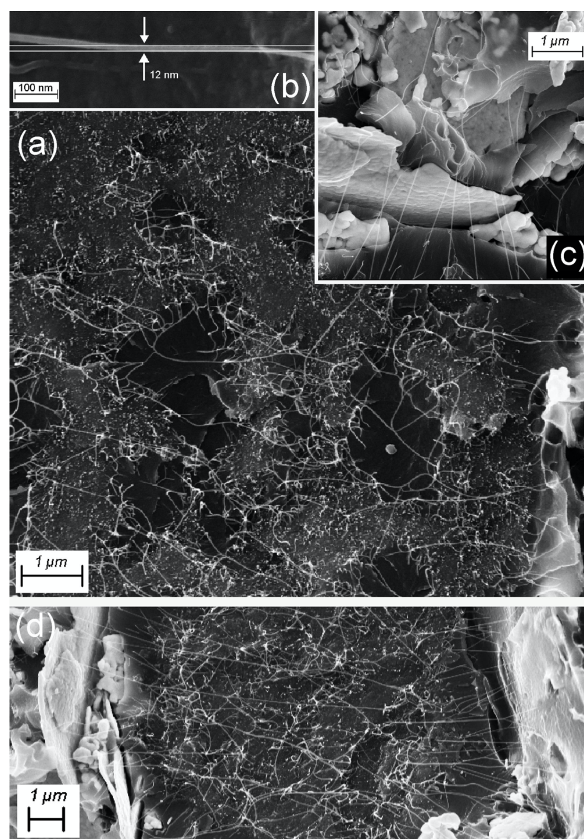

Figure 2: (a) SEM image of a nanotubes silver-filled epoxy nanocomposite prepared with DWNT at a concentration of 1% w/w. (b) Zoom on a single nanostructure showing a bundle ~ 1 μm long with diameter of 12nm. Zooms on different parts of the sample highlight how the CNTs interconnect silver platelets closely spaced (c) and distant apart (d) through the epoxy matrix.

The CNTs average length is in the micron range. Shorter fragments with lengths of some hundreds of nm are also observed (spotted zones in Figure 2a). The average tubes diameter is within 10 – 15 nm (Figure 2b) which, according to the nominal diameter of the single tubes, suggests the presence of bundles containing ~ 5 – 15 nanotubes each. As shown by the SEM images the CNTs, on one hand, interconnect the different areas of the resin, partially filling the micrometric holes likely produced during the solvent evaporation (darker zones in Figure 2a); on the other hand, they foster the contact among closely spaced silver platelets (Figure 2c) and, finally, result in a conductive network capable of interconnecting silver platelets located far apart (Figure 2d).

GNP characterization and Morphology of the GNP-added composite

Figure 3a displays the absorption spectrum of GNPs after sonication of 1 mg of graphite in 40 mL of IPA (0.01% w/w with respect to the resin). It highlights the UV peak due to the van Hove singularity of the graphene density of states,[49] with a long featureless tail related to the linear dispersion of the Dirac electrons. Using the absorption coefficient $\alpha = 3620 \text{ mL mg}^{-1} \text{ m}^{-1}$ taken from ref. [47,50] we estimate a graphene concentration of 0.015 mg/mL. MicroRaman spectroscopy is exploited to estimate of the number of layers present in the graphene platelets.[51] Measurements are carried out at 515nm after drop casting on a Si/SiO_2 substrate and solvent evaporation. Figure 3b compares the HOPG spectrum (blue) with a representative spectrum of the graphene flakes (light red, red). The main D, G and 2D bands are visible. The D band originates from the breathing mode of the sp^2 rings and requires defects to be activated.[51] It is dispersive with the excitation wavelength and we find it around 1340 cm^{-1} for 515nm excitation on the graphene flakes, whereas it is negligibly small in the starting HOPG. The G-peak is due to bond stretching of sp^2 atoms (E_{2g} phonon) and its position is found around 1580 cm^{-1} in both graphene and graphite. The 2D band is the second order of the D peak. It is dispersive with the excitation wavelength and located ~ 2700 cm^{-1} for excitation at 515nm.[51] It is a single peak for single layer graphene and consists of two components in bulk graphite. [51] For high purity micromechanically cleaved samples, the 2D band splits into several components and its shape allows one to distinguish among 2, 3, 4, 5 and >10 layers (bulk graphite). The Raman spectrum of graphene produced by LPE is more difficult to interpret. Staking faults, edge effects, strain and doping don't permit to unambiguously determine the number of layers present in a flake. In our spectra the 2D band of graphene platelets is different from graphite and consistent with graphene platelets containing single (red line) and few layers (violet line) of graphene with random staking upon aggregation subsequent to IPA evaporation.[52,53] In figure 3b we also labeled the D' peak, that, as the D band, is a defect induced Raman line generated by TO phonons at the corner K of the Brillouin zone, and interpreted as a double resonance mechanism here connecting two points of the same Dirac cone around K (intra-valley

process).[51] In carbon materials an increase of the $I(D)/I(G)$ ratio is indicative of defect formation. In LPE graphene defects can be due to both disorder localized at the edges or disorder in the bulk of the samples. [53] Ref. 47 has reported that exfoliation in IPA yields good quality graphene flakes and that the increased D band is due to the disorder induced by the creation of new edges. Here we find an increase of the $I(D)/I(G)$ ratio from 0.03 in HOPG to 0.3 in graphene. The difference, $\Delta[I(D)/I(G)]$, can be used to get an estimate of the flakes dimensions[47] through the relation $[\langle L\rangle^{-1} + \langle w\rangle^{-1}] = 15.4 \times \Delta[I(D)/I(G)]$ where $\langle L\rangle$ and $\langle w\rangle$ are the average length and width of the flakes measured in μm. The value $\Delta[I(D)/I(G)] = 0.27$, according to the experimental data reported in ref. [47], corresponds to $[\langle L\rangle^{-1} + \langle w\rangle^{-1}] = 3 \div 5\ \mu m^{-1}$, i.e to micrometric flakes.

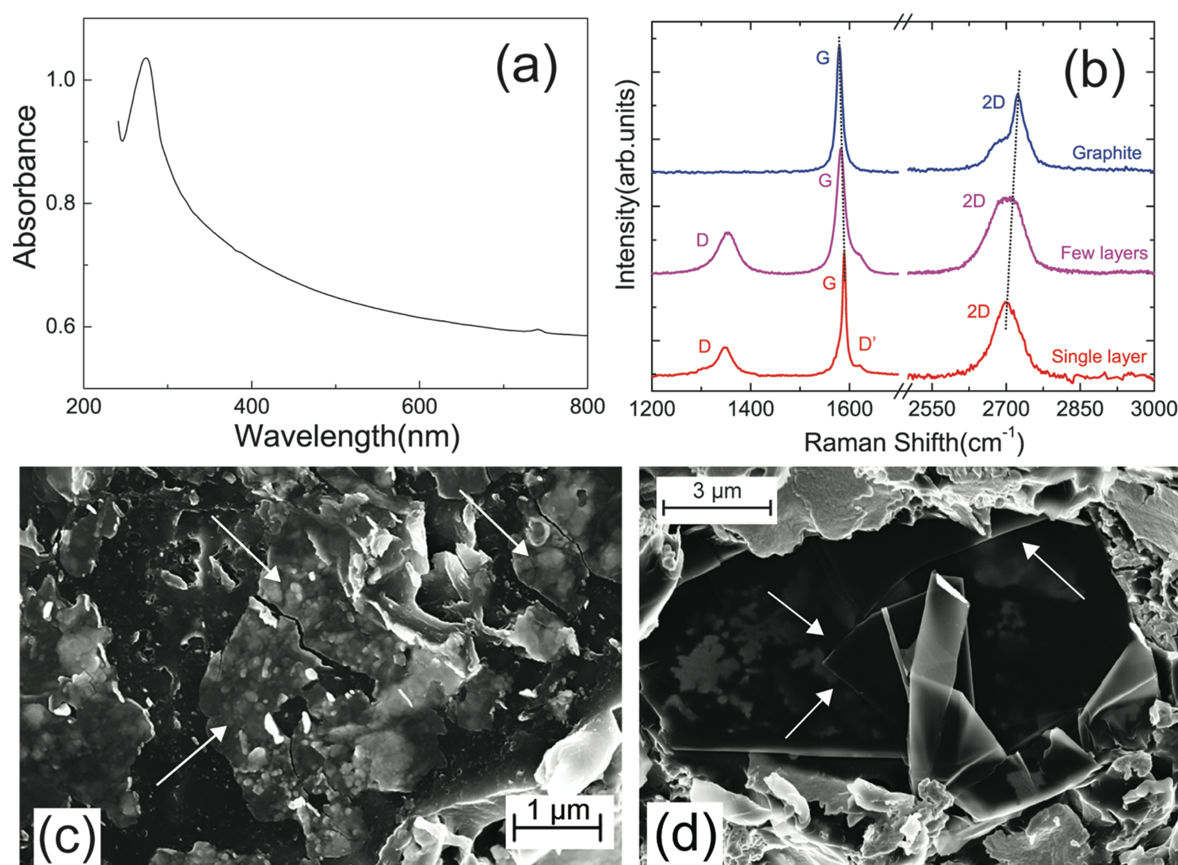

Figure 3: (a) Absorption spectrum of the graphene solution. (b) Raman spectra of HOPG (black line) and of few layers (violet line) and single layer graphene platelets (red line). (c, d) SEM images of the GNPs-filled nanocomposite. Indented graphene flakes interconnect the silver particles. Large flakes are also visible in which the straight edges (d, arrows) highlight the staking among the flakes.

Figure 3c shows the SEM image of a nanocomposite prepared with graphene, highlighting flakes with dimensions of few microns embedded among the silver particles. The flakes' edges are indented. On some sparse zones of the sample there are larger flakes (d), locally wrinkled. The straight edges (arrows in Figure 3d) mark the separation among flakes with different number of layers and highlight the staking of the flakes. As for the nanotubes, SEM analysis indicates that graphene interconnects the metal particles improving electron and heat conduction with respect to the metal-metal point contact.

Thermal and electrical properties of the CNTs-added nanocomposites

Figure 4 displays the thermal conductivity (a) and the electrical resistivity (b) of the nanocomposite prepared with DWNTs at increasing concentrations. Up to ten samples are prepared for each concentration and a box-whisker plot is used to display the data distribution. The measured thermal conductivity of the epoxy as purchased is $K_T = 2.6 \pm 0.1$ W/mK, in agreement with the specifications. Treatment with pure IPA (no addition of carbon nanostructures) does not produce any appreciable change, but for a slight worsening ($K_T = 2.4 \pm 0.3$ W/mK). Adding 0.01% w/w and 0.5% w/w of DWNTs we start seeing some improvement of the thermal conductivity with maxima value of 4 W/mK. At 1% w/w we observe a strong increase of K_T up to a maximum of 10.5 W/mK. The median of the conductivity found on more than 10 different samples is 8 W/mK. Increasing the nanotubes quantity we observe a worsening of the thermal conductivity with a maximum (median) value of 5.0 W/mK (4.5 W/mK) for 2 %w/w of DWNTs, down to 3.2 W/mK (3.0 W/mK) for 4 %w/w content. Concerning the electrical resistivity, the pristine epoxy shows an average value of $\rho = 350 \pm 30$ μΩ cm, in agreement with the specifications. Treatment with pure IPA (no addition of CNTs or GNPs) produces a worsening of the conductivity, with values that can go from 400 to 800 μΩ cm. Addition of 0.01% w/w and 0.5% w/w of DWNT yields a slight decrease of the resistivity with average values between 300 and 275 μΩ cm, and best values of 190 μΩ cm. Again, addition of 1% w/w DWNTs yields a remarkable decrease of the resistivity with

measured minima values of 50 μΩ cm. The median value measured over 16 samples is $\rho =$ 110 μΩ cm. Increasing the nanotubes quantity we see a worsening of the electrical conductivity, but less marked than the thermal conduction. Resistivity increases to a best (median) value of 90 μΩ cm (130 μΩ cm) for DWNTs 2% w/w, 110 μΩ cm (140 μΩ cm) for DWNTs 3% w/w, up to 290 μΩ cm (320 μΩ cm) for DWNTs 4% w/w.

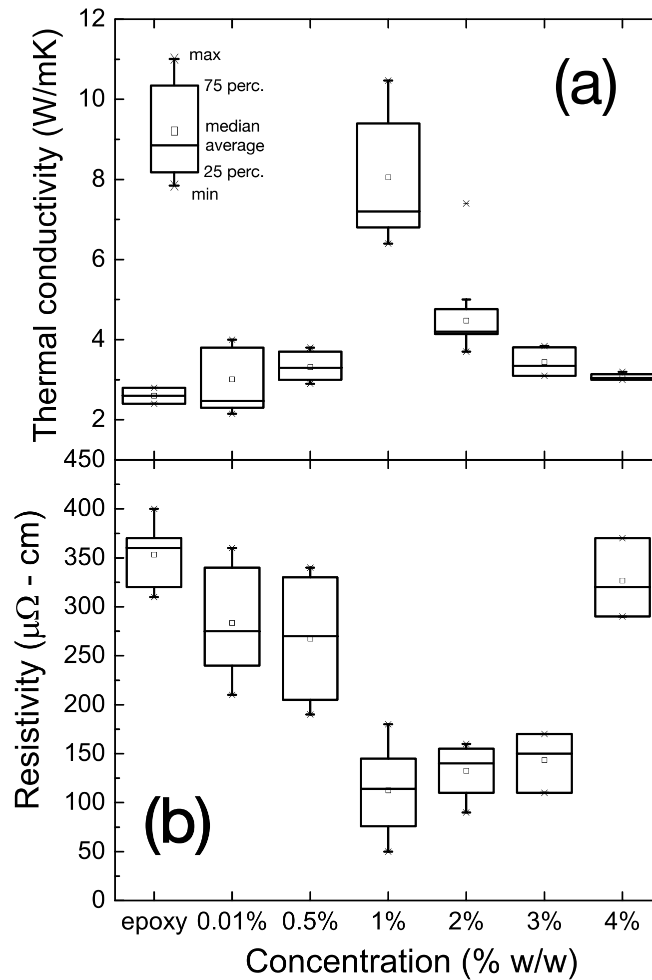

Figure 4: Plots of the thermal conductivity (a) and electrical resistivity (b) of the DWNT-added nanocomposite as a function of the CNT weight concentration. Up to ten samples were investigated for each concentration. The box-whisker diagrams summarize the statistical distribution of the dataset, displaying the 75th and the 25th percentile, the median, the average, the maximum and the minimum values, as highlighted by the legend in (a).

Comparative experiments with DWNTs functionalized with COOH and NH_2 groups, and MWNTs featuring micrometric length have been aimed at investigating the maximum thermal conductivity that can be reached with our methodology. The loading (1% w/w), the solvent (IPA) and the dispersion parameters (sonication power and time) are left unchanged. Figure 5(a) shows that, while pure DWNTs allow one to overcome 10 W/mK, DWNTs functionalized with COOH and NH_2 groups, as well as MWNTs, yield an improvement of K_T up to a maximum of ~ 4 W/mK. A parallel SEM analysis highlights that, while the pure DWNTs nanocomposites show the presence of networks with micron long tubes (Figure 5b), the functionalized DWNTs are indeed well homogenized with the resin (c, d) but the tubes are broken into fragments few hundreds of nm long.

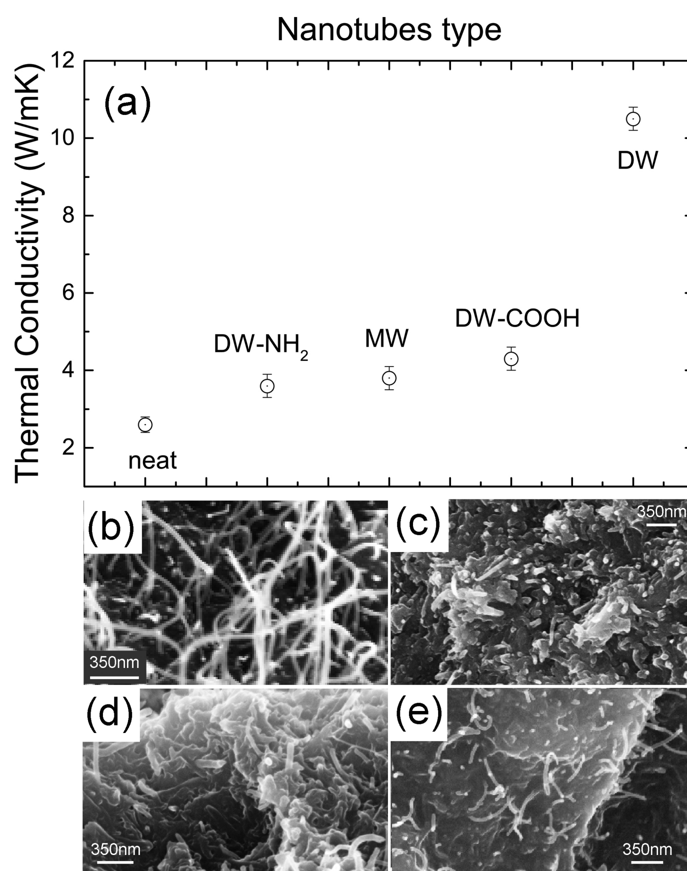

Figure 5: (a) Maximum thermal conductivity measured using different types of CNTs 1% w/w, dispersed in IPA. SEM images showing typical morphologies of the resin added with pure DWNTs (b), DWNT-COOH (c), DWNT-NH_2 (d) and MWNT (e).

The thermal-interconnection role played by the CNTs, in this latter case, is expected to be strongly depleted and this could justify the smaller K_T measured. The same effect is observed with MWNTs (Figure 5e) and when using THF to disperse the DWNTs (image not shown). This analysis suggests that, together with the dispersion efficiency, the average length of the CNTs networks in the nanocomposite can be an important factor for the improvement of the conduction properties of the nanocomposite, in agreement with previous observations on CNT-polymer systems.

Thermal and electrical properties of the GNP-added nanocomposites

Our study with graphene has been motivated by the exigency to find a feasible way of improving both the electrical and thermal properties using GNPs at minimum loading possible. We have therefore focused our analysis on graphene-added nanocomposites starting from concentrations down to 0.001% w/w, i.e. 50 times smaller than those used by Liu et al.[41] As shown in Figure 6a, at 0.001% w/w there is a slight worsening of the thermal conductivity (2 W/mK), whereas at 0.005% w/w the conductivity starts improving with an average value of 4.0 W/mK. Notably, K_T can be increased up to a maximum of 11.8 W/mK using 0.01% w/w of GNPs. The average conductivity measured over ten samples is 9.5 W/mK. A remarkable improvement of the thermal conductivity is observed also at concentrations of 0.03 and 0.06% w/w (maxima values of 8.6 and 10.6 W/mK, median values 6.5 and 8.5 W/mK). Increasing the quantity of GNPs to 0.2% w/w and, beyond, to 1% and 3% w/w we observe a reduction towards values comparable with the conductivity of the pristine resin, as for the DWNTs. From the electrical point of view, the best electrical resistivity is also found for 0.005% w/w GNP concentration and amounts to 30 μΩ cm (Figure 6b), i.e. one order of magnitude better than the neat epoxy. The average value over ten different samples is 65 μΩ cm. At lower concentrations (0.001% w/w) the resistivity is similar to the neat epoxy value (average 340 μΩ cm), while at higher concentrations (0.01 and 0.03 % w/w) the resistivity is again, much improved (best values of 35 and 70 μΩ cm, average values of 70 and

85 μΩ cm). Further increasing the concentration we see, again, a gradual worsening of the average electrical conductivity towards resistivity values comparable or even higher than the neat resin (values up to 500 μΩ cm are measured for 1 and 3% w/w).

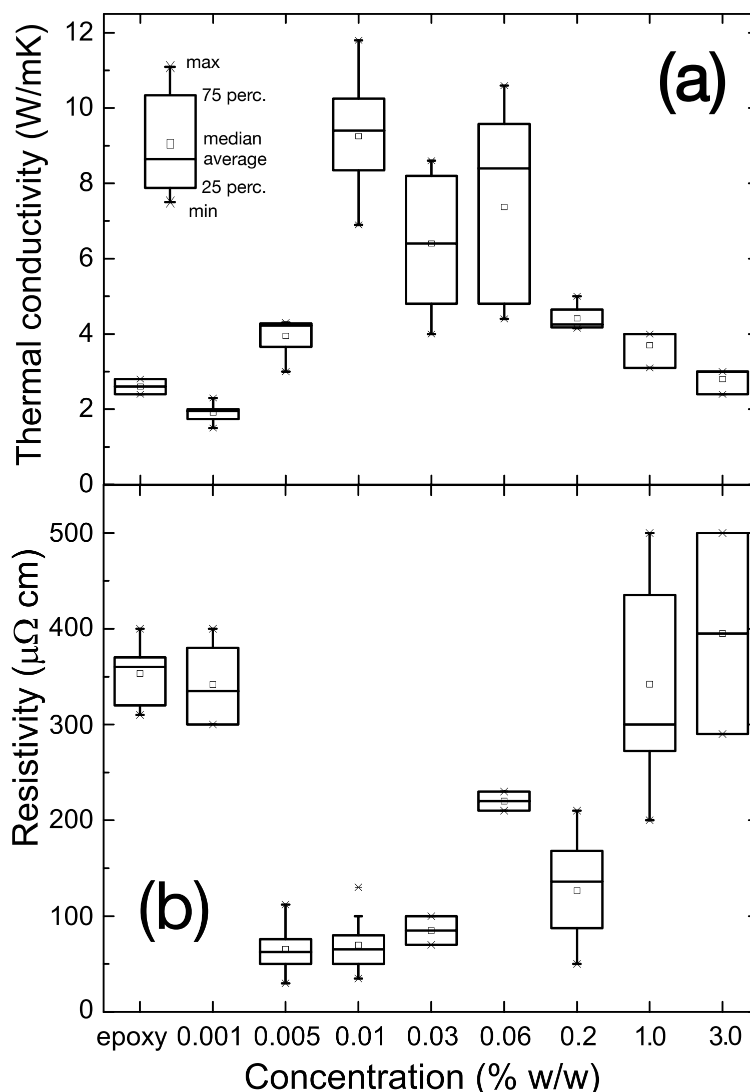

Figure 6: Plots of the thermal conductivity (a) and electrical resistivity (b) of the GNPs-added nanocomposite as a function of the weight concentration.

Figure S2 (Supporting Information) summarizes the results obtained with CNTs and GNPs. GNPs permit to reach ca. 10% higher thermal conductivity than DWNTs for what concerns the best measured value (11.8 W/mK against 10.5 W/mK) and the average value over more than 10 samples

(9.2 W/mK against 8 W/mK). From the electrical point of view GNPs yield a conductivity increase more than 30% better than DWNTs. The minimum resistivity found with GNPs is, in fact, 33 μΩ cm, against 50 μΩ cm with DWNTs. The average resistivity values found with GNPs and DWNTs are, respectively 68 and 124 μΩ cm. A further comparison is shown with samples synthetized by adding an equivalent amount of HOPG fragmented into micrometric pieces by manual grinding in an agate mortar. With HOPG we find an increased thermal conductivity up to ~ 5 W/mK. The electrical resistivity is, conversely, worsened. These results highlight the importance of having nanoscale structures, as graphene and CNTs, intercalated among the polymer cross-links in order to achieve optimal thermal and electrical conductivity. The better conductivity observed with GNPs is likely to be attributed to the larger area exposed for contact with metal platelets. Finally, graphene is advantageous because of the much smaller quantity of filler needed, c.a. 100 times less than DWNTs, and the lower costs of graphite with respect to commercial CNTs.

Curing, viscosity and die shear tests

We have used Differential Scanning Calorimetry (DSC) to monitor the cure kinetics of the neat adhesive and of the nanocomposite. DSC measures the heat flow associated with transitions and chemical reactions of a sample undergone to a temperature profile as a function of time, and permits to determine the temperature at which these processes occur. Figure 7(a) compares the kinetic profiles of three uncured samples of neat (red line), DWNTs-added (blue line, 1% w/w) and graphene-added epoxy (black line, 0.01%w/w) subjected to a controlled temperature ramp. A single exothermic peak is observed on all the samples in the temperature range studied (60 – 250 °C), indicating that the fastest cure occurs at T_{curing} ~ 140 – 145 °C (143 ± 5 °C for the nanocomposite against 140 ± 5 °C for the neat epoxy). The curing onset is located at ~ 130 °C (inset of Figure 7a). The absence of any further feature in the thermodynamic curing profiles confirms that the nanocarbon-added composites are stable up to temperatures of 250 °C. DSC has also been used to determine how long the resin takes to completely cure at a given temperature. The isothermal curing

profiles shown in Figure 7b show that at 135 °C, i.e. between the onset and the fastest curing temperature, the curing is completed in ~ 15 min (red dashed line) for neat epoxy and ~ 5 min (red line) for graphene-added epoxy (0.01% w/w), while at 90 °C (black dashed line) the curing is completed after ~ 55 min for neat epoxy and ~ 40 min for graphene-added epoxy.

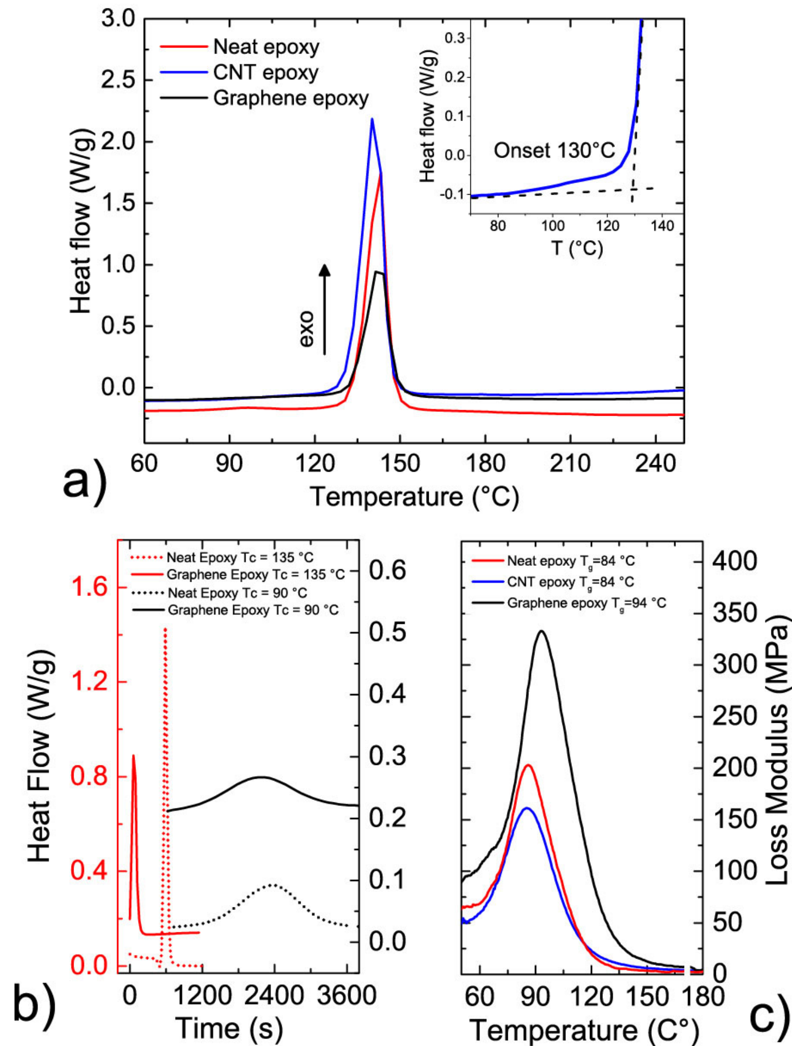

Figure 7: (a) Curing profile of the neat epoxy (red line), the 1% w/w DWNTs-added nanocomposite (blue line) and of the graphene-added nanocomposite (black line). The inset highlights the onset of the curing process at ~ 130 °C. (b) Isothermal curing profiles at T = 90 and 135 °C (black and red lines). Data are normalized to the weight of the sample. (c) Glass transition temperatures measured for the neat epoxy (red) and the 1% w/w DWNTs-added epoxy (blue) and 0.01% w/w graphene-added nanocomposite (black line) measured with DMA at 1Hz.

The acceleration of the curing reaction in presence of GNPs, probably, has to be attributed to the high thermal conductivity of the GNPs that, fostering a better heat propagation inside the sample, catalyzes and speeds up the process.[54]

Conductive adhesives, as other cross-linked materials, when re-heated after curing do undergo a very slight softening at a point known as the glass transition temperature (T_g). We have used Dynamic mechanical analysis (DMA) to monitor the T_g of the three samples. The T_g of the neat epoxy and DWCNT systems (Figure 7c) are found to be comparable at ~ 84 °C, while the T_g of the graphene-added epoxy (black line, 0.01% w/w) is 94°C. Our measurements show that the introduction of small quantities of DWNTs and graphene does not change appreciably the polymerization process, and that the thermodynamic parameters are almost unchanged with respect to the neat epoxy. The viscosity of the resin added with carbon nanostructures has been measured at room temperature and is found to be slightly (10%) higher than the neat epoxy. Such a small viscosity increase with respect to other reports[55] can be explained by the solvating effect of the IPA expected to weaken the inter-chain interactions.[56]

Die shear strength is a test used to determine the grip of a component bonded to a package substrate using an attach adhesive. The component is subject to an increasing stress parallel to the substrate up to its detachment (see sketch in Figure 8a), providing a quantitative measure of the maximum shear stress that the adhesive interfaces can sustain. Die shear strength varies significantly with the die size, therefore we have analysed two standard SMD components with different areas, namely 63×10^{-4} in^2 (Figure 8b) and 39×10^{-4} in^2 (Figure 8c), bonded to gold substrates. For both components we compare the performances of the normal resin (red bars), the DWNT-added (blue bars) and the graphene-added nanocomposite (green bars) after curing (left) and after 240 thermal cycles between -55 and 125 °C (right). On the 63×10^{-4} in^2 components the measured die shear forces are higher than 5 Kg with both the nanocomposites even after the thermal cycles, i.e. well above the MIL-STD-883 limit (see Figure S3 in Supporting Information). On the 39×10^{-4} in^2, after curing, the neat epoxy features a maximum loading of 4.6 Kg, the DWNT-

nanocomposite gives 2.5 Kg and the graphene-added resin 3.5 Kg. After thermal cycles the maximum loadings decreases to 1.8 Kg and 2.9 Kg for the DWNT- and graphene- added resins, respectively. These values are smaller than the neat epoxy (4.8 Kg) but still satisfy the MIL-STD-883 requirements (1.5 Kg, see Figure S3 in Supporting Information).

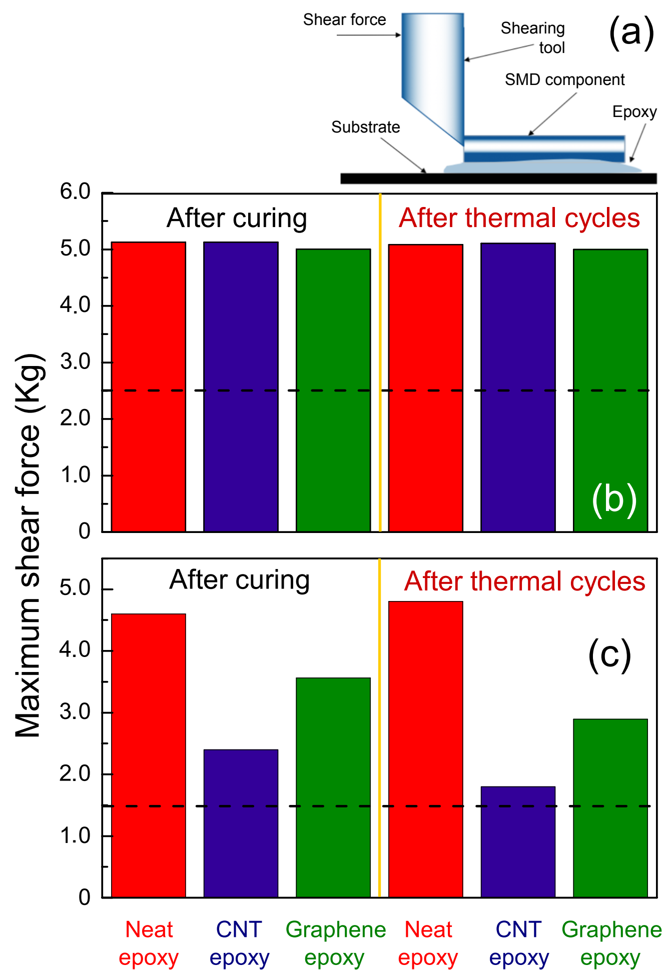

Figure 8: (a) Schematic of the die shear test: a tool applies a shear force to the die component attached to the substrate through an epoxy layer. Maximum die shear forces measured: (b) on 63×10^{-4} in^2 and on (c) 39×10^{-4} in^2 SMD components bond to gold substrates using the neat epoxy (red bars), the DWNTs-added nanocomposite (blue bars) and the graphene-added nanocomposite (green bars). Results are presented after curing and after subsequent 240 thermal cycles between -55 and 125 °C. The dashed lines indicate the minimum performance loadings required by the MIL-STD-883 (2.5 Kg and 1.5 Kg, respectively, see Figure S3).

Finally, a different commercial-grade two-components Ag paste based on Bisphenol A Diglycidyl Ether and functionalized acrylate is investigated to confirm the possibility of using our methodology for the simultaneous improvement of the conduction properties on a high conductivity and more viscous adhesive (6000 cP). According to the specifications the adhesive has a resistivity $\rho \leq 80$ μΩ cm and a thermal conductivity K_T = 11.9 W/mK. The measured values on the resin as purchased are ρ = 75±5 μΩ cm and K_T = 8.9±0.4. No information on the silver content has been provided by the manufacturer. The same procedures described previously are used to add 1% w/w of DWNTs and 0.01% w/w GNP to the resin and to investigate the nancomposite conductivity. Curing is carried out at 150°C for 1h. We find that with DWNTs the average resistivity is decreased down to 28±8 μΩ cm with a minimum value of 19 μΩ cm. Using graphene we find even better results with an average resistivity of 23±8 μΩ cm and minimum values of 9 μΩ cm, and an increased thermal conductivity of 18.1 ± 0.8 with maximum measured values of 19.4 W/mK.

Temperature of GaN transistors bonded with the nanocomposites

Performance tests of the nanostructured resin have been carried out by measuring the temperature reached by GaN-based MMICs (Figure 9a) operating in the frequency range of 9-10 GHz (the X band) bonded into RF power amplifier circuits using DWNT- and graphene- added epoxies, comparing the results with the pristine resin. The test jig is shown in (Figure 9b). The amplifiers are biased with a voltage of 30 V and a current of 1.5 A through 50 Ohm resistors. No RF signal is injected. In such conditions maximum heating is expected. We apply infrared thermography to compare maximum, minimum and average temperatures of circuits bonded with different resins. Figure 9c shows the thermal map of a GaN MMIC bonded with a nanostructured resin. Higher temperature zones (T > 100 °C, in yellow colour) can be seen all around the chip, where maximum power is dissipated. Similar temperature distributions are observed on all the circuits, independently from the epoxy used for bonding. Remarkable differences are instead observed for what concerns the maximum and the average temperature reached by the MMICs. Figure 9d summarizes the

results. Whereas with the pristine resin we measure peak temperatures in the 155 – 160 °C, and average temperatures around 90 °C, the use of nanostructured resins allows to reduce the peak temperature by 20 – 30 °C (~ 125 °C with CNTs and ~ 135 °C with graphene) and the average temperature by ca. 10 °C. This change is significant considering that a hotspot temperature reduction by ~20 °C can correspond to an order of magnitude increase in the MTTF of GaN integrated circuits. [19]

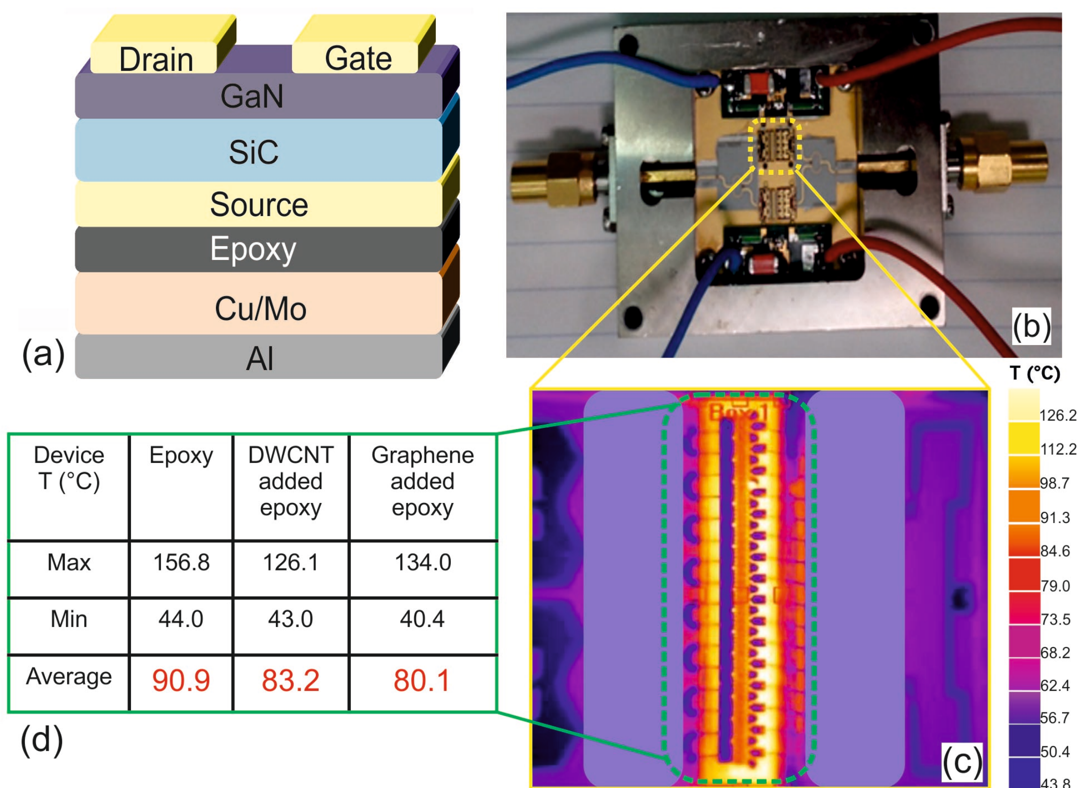

Device T (°C)	Epoxy	DWCNT added epoxy	Graphene added epoxy
Max	156.8	126.1	134.0
Min	44.0	43.0	40.4
Average	90.9	83.2	80.1

Figure 9: (a) Schematic of the GaN MMIC assembled in the power amplifier. (b) Photograph of a device in which two MMICs are mounted in parallel (the dotted line highlights one of them). (c) IR image of the GaN MMIC under biasing conditions. The temperature is reported in a false colours scale with the yellow zones characterized by the highest temperatures and the blue zones by the lowest. (d) Table reporting the minimum, maximum and average temperature reached by the device.

DISCUSSION

We have shown that the addition of pure DWNTs and GNPs to silver-filled conductive adhesives yields a remarkable improvement of both the electrical and thermal conduction properties. Here we discuss in more detail some specific issues regarding the low volume fraction of CNTs and GNPs at which a large conductivity increase occurs and the observation of an optimal concentration value beyond which the conductivity worsens, and to draw some conclusions on the role played by graphene and CNTs in the conduction improvement. Before addressing these points let us remind the conductivity mechanisms of CAs.

Electrical conduction in CAs

Conductive adhesives are two-components formulations prepared by mixing polymeric resins that are insulating, with metallic fillers that are conductive. The filler provides the conductivity properties (transport of heat and electrical current) while the polymer provides the mechanical properties (adhesion). CAs are generally insulators before cure. The conductive metal platelets are, in fact, totally surrounded by the polymeric resin and/or lubricant layers with no platelet-to-platelet contact (see sketch in Figure 10a). High conductivity is achieved only after curing, when the polymeric matrix shrinks due to the formation of chemical cross-links among the polymer chains.[5] The compressive stress pushes the metal platelets close together, contacting them and enabling electrons to flow through the metal filler. The metal platelets "touch" each other at the so-called contact points (Figure 10c), regions through which electrons flow. Conduction occurs via tunnelling through thin layers of residual polymer surrounding the metal platelets and/or through nanometric-scale contacts between adjacent platelets. Percolation theory[57] has been used to explain conduction of ECAs. Once the filler volume fraction, f, overcomes the percolation threshold, f_c, which typically occurs at metal volume concentrations of 15 – 30 %, a significant number of percolation paths are formed (as sketched in Figure 10b). Percolation leads to a dramatic increase of the electrical conductivity according to the typical law $\sigma \propto [(f - f_c)/(1 - f_c)]^2$ for 3D systems.

Several computational models have been developed to understand the conductivity of composites filled with both spherical and non-spherical metal particles.[58,59]

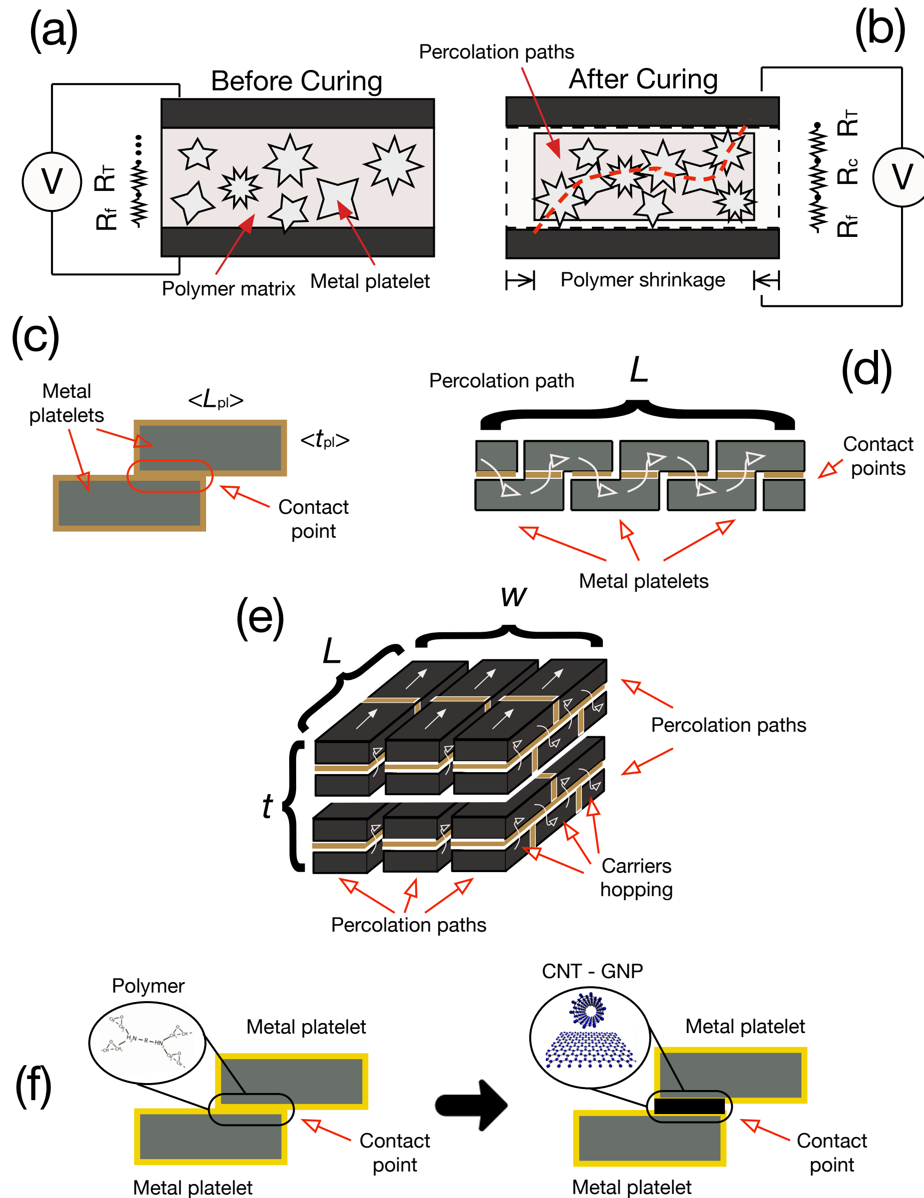

Figure 10: Schematic of ECAs before (a) and (b) after curing. R_f : intrinsic metal platelet resistance; R_T : tunnelling resistance; R_c : constriction resistance. (c) Sketch of the platelets arrangement into overlapping pairs and (d) of the arrangement of the platelets-pairs to form the percolation paths. (e) Arrangement of the percolation paths into the final sample (length L, width w, thickness t). (f) Upon addition of carbon nanostructures, electron conduction at the contact points is modified from tunnelling through the polymeric layer to an ohmic contact mediated by the CNTs/GNPs.

In order to predict the resistivity of our resin and get insight on the mechanisms ruling the electrical conduction, we have re-formulated the model proposed by Rushau et al.[58] to the case of resin filled with rectangular metal platelets. Details of the calculations are reported in Note 1 of the Supporting Information. Briefly, we model our sample as a set of metal platelets with average lateral dimension $<L_{pl}>$ and thickness $<t_{pl}>$ (see Figure 10c). These are staked into pairs with a surface overlap (contact area) equivalent to 50% of the lateral area, in a close packed arrangement. The platelets-pairs add up to form the percolation paths (Figure 10d), i.e. conductive chains that extend all along the sample length (L = 7cm). The carriers flow inside these chains by jumping from one platelet to the other. The final sample (Figure 10e) is modelled as a network of percolation paths ordered parallel the one to the other along its width (w = 4 mm) and thickness (t = 60 μm). Such assumptions are based on the section and in-plane SEM images (Figure S1a,b in Supporting Information) showing the alignment and superposition of the metal platelets. Based on this model, the sample total resistance, R_{sample}, can be calculated as the parallel of N_{paths} conduction paths, each composed by a series of N_{pl} resistive metal platelets-pairs, each one having resistance R_{pl}. The resistance of each pair, R_{pl}, is the sum of the intrinsic resistance (ohmic resistance given the metal) and the contact resistance (the tunnelling resistance plus the constriction resistance due to conduction through the residual polymer layer and nanoscale contacts). The resistance of each percolation path will be $R_{chain} = \sum_{pl}^{N_{pl}} R_{pl}$, the sample total resistance $R_{sample}^{-1} = \sum_{path}^{N_{paths}} 1/R_{path}$. The number of platelets-pairs in each path, N_{pl}, as well as the number of percolation paths in the sample, N_{paths}, can be estimated from geometrical considerations based on the filler fraction and on the platelets and sample dimensions. After calculations (see Note 1 in Supporting Information) the effective sample resistivity turns out to be

$$\rho_{eff} = \langle R_{sample} \rangle (wt/L) = 2\big(\langle t_{pl} \rangle / f_{Ag}\big) \times [\rho_f / \langle d \rangle + \rho_t(t_m)/\langle a \rangle] + \rho_f / f_{Ag} \quad (1)$$

where f_{Ag} is the filler volume fraction, ρ_f the filler resistivity, $\rho_t(t_m)$ the tunnelling resistivity as a function of the polymer layer thickness, t_m, $\langle d \rangle$ is the average contact point diameter and $\langle a \rangle$ the

average contact point area. For the calculations we can reasonably assume that $\langle d\rangle \sim \sqrt{\langle a\rangle}$. Eq. 1 contains two terms. The first, $\rho_{\text{contact}} = 2\left(\langle t_{\text{pl}}\rangle / f_{\text{Ag}}\right) \times [\rho_{\text{f}}/\langle d\rangle + \rho_{\text{t}}(t_{\text{m}})/\langle a\rangle]$ is related to the contact resistivity, given by the sum of the constriction and the tunnelling contributions, respectively. The second term, $\rho_{\text{intrinsic}} = \rho_{\text{f}}/f_{\text{Ag}}$, is related to the intrinsic filler resistivity. ρ_{eff} decreases at increasing filler fractions, as expected. ρ_{eff} depends on the average contact area, $\langle a\rangle$, and contact diameter, $\langle d\rangle$ among the platelets, decreasing when these two parameters are larger. Contact area and contact diameter are related to the intrinsic pressure exerted by the polymer matrix on the metal platelets after curing and whose effect is to bring the platelets into contact. The internal stress mainly origins from: thermal stress, generated when the composite is cooled down, after curing, because of the different thermal expansion coefficients of polymer and filler; stress induced by the epoxy shrinkage due to formation of cross-links among the polymer chains.

We compare the predictions of Eq. 1 with our experiments starting from the neat resin. This latter, we remind, is a binary mixture of silver (resistivity ρ_{f} = 1.6 μΩ cm) in form of micrometric platelets, dispersed in an epoxy matrix (typical resistivity $\rho_{\text{m}} \sim 10^{12} - 10^{16}$ Ω cm).[31,60] The density of the resin is 2.67 g/cm^3. The silver mass fraction is 78%, corresponding to a volume fraction f_{Ag} = 20%, calculated using the equation $f_{\text{Ag}} = m_{\text{Ag}}/\left[m_{\text{Ag}} + \left(\delta_{\text{Ag}}/\delta_{\text{m}}\right)\left(1 - m_{\text{Ag}}\right)\right]$ where m_{Ag} is the filler weight fraction, δ_{Ag} is the filler density (10.5 g/cm^3) and δ_m the polymer matrix density (0.73 g/cm^3). The average lateral dimension and thickness of the platelets, $<L_{\text{pl}}>$ = 4.2 μm and $<t_{\text{pl}}>$ = 200 nm, are estimated from the SEM images (Figure S1 in Supporting Information). The SEM particles images, shown in Figure S4 (Supporting Information), display the presence of platelets with lateral dimensions from 1 μm to ~ 15 μm. The spread of the thickness is of the order of 50nm. After curing, the composite reaches a resistivity $\rho = 350 \pm 30$ μΩ cm. Considering that the silver volume fraction is 20%, i.e. 1/5 of the total volume, the minimum effective resistivity that we could expect (if all the silver platelets were ideally concentrated in a single conducting wire) would be $\rho_{\text{intrinsic}} = \rho_{\text{Ag}}/f_{\text{Ag}}$ i.e. 8 μΩ cm., as predicted by the third term in Eq. 1. The fact that the

measured effective resistivity is more than 40 times higher (350 μΩ cm) is the consequence of the fragmentation and non-zero contact resistance of the metal platelets, giving rise to a relevant tunnelling and constriction resistivity, whose effects are described by the first term of Eq. 1.

We analyse two different physical scenarios. The first one, in which the metal platelets after curing are still covered with a residual polymer layer 1nm thick. Following Ruschau et al.[58], this corresponds to a tunnelling resistivity of $\rho_t = 10^{-7}\ \Omega\ \mathrm{cm}^2$ (Figure S5 in Supporting Information). In the second scenario, after curing, we assume physical contact among the metal platelets through nanoscopic contact points. In this latter picture the tunnelling resistance is neglected and the constriction resistance rules the conduction. Lu et al. [6] and Kim et al.[58] assumed such a hypothesis in their computations.

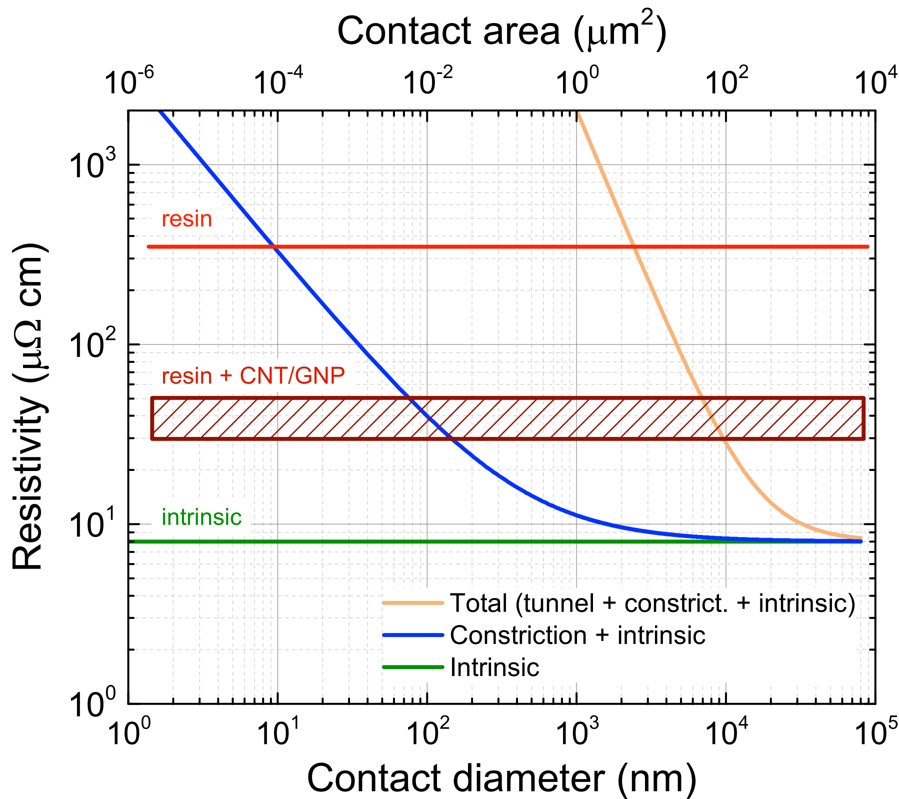

Figure 11: Plots as a function of the contact diameter and of the contact area (top axis) of the total effective resistivity (orange line), i.e. tunneling + constriction + intrinsic, of the constriction + intrinsic component (blue line) and of the intrinsic resistivity (green line). The red line indicates the resistivity of the pristine resin. The dark red dashed box indicates the resistivity of the CNT/GNPs added composite.

In Figure 11 we plot the different resistivity contributions (total, constriction and intrinsic) as a function of the contact diameter and area. The total resistivity (orange line), which includes tunnelling, constriction and intrinsic resistivity, turns out to be orders of magnitude larger than the constriction + intrinsic resistivity contribution (blue line). This suggests that, in a physical picture in which the metal platelets are covered by some residual polymer layer, the sample resistivity is ruled by the tunnelling contribution. Ruschau et al.[58] reached analogous conclusions for closely packed spherical particles. The total resistivity is observed to decrease from ~ 10^3 μΩ cm down to the intrinsic resistivity for the resin, $\rho_{\text{intrinsic}} = 8$ μΩ cm (green line), when the contact area among the platelets increases from 1 to 10^4 μm^2. This model well describes the resistivity value of our neat resin (350 μΩ cm, red line in Figure 11), suggesting an average contact area of ~ 6 μm^2. Such value is slightly smaller but in agreement with the assumptions of maximum platelet overlap (50% of the platelet area) corresponding to $1/2\ \langle L_{\text{pl}} \rangle^2 \sim 8.5\ \mu\text{m}^2$. Notably the model sets a limit of ~ 200 μΩ cm to the minimum resistivity reachable with the metal platelets sizes present in our resin, and that the limit is reached when the contact area is exactly $1/2\ \langle L_{\text{pl}} \rangle^2$.

In the second physical picture, in which conduction occurs through localized nanometric contact points and the tunnelling resistivity is neglected, the resistivity (constriction + intrinsic) is observed to decrease from ~ 10^3 μΩ cm to the intrinsic value (8 μΩ cm) for contact point diameters increasing from 1nm to 10 μm (Figure 11, blue line). Also this model can describe the resistivity value found on our neat resin, suggesting an average contact point diameter of 10nm. Differently from the tunnelling conduction, the contact-point conduction can account for resistivity values lower than 100 μΩ cm of the neat resin, provided that the contact point diameter is larger than some tens of nanometres. We are not able, at this stage, to draw a definitive conclusion on which of the two scenarios rules the conductivity in our resin. The theoretical model, however, clearly indicates that resistivity values below 100 μΩ cm cannot be reached in a picture in which the platelets are

covered by a polymeric layer, requiring necessarily an enhanced physical contact among the metal surfaces.

Indeed, the assumptions made in our toy model include some strong approximations.

(i) The arrangement of the metal platelets in the real sample shown in Supporting Figure S1 is indeed more complex than the one we have assumed in Figure 10(e). In the model we don't take into account the presence of smaller nano-particles and we do not consider possible misalignment of the platelets. The addition of small filler nanostructures generally increases the electrical conductivity due to sintering effects increasing the contact area among platelets. On the other hand, misalignment among the metal platelets results in a decreased contact area and a consequent worsening of the conductivity. We suppose that our model is capable to correctly predict the value of the resin resistivity because the small filler nanoparticles and platelets misalignment produce effects that counterbalance in the real sample. Misalignment effects, in particular, are expected to influence particularly the predictions in the tunnelling conductivity picture, in which large contact areas are needed (micron scale) to explain the resin resistivity. In the nanoscale contact picture, where the predicted contact diameters are as small as 1nm, we do not expect such a big influence.

(ii) We assume that all the particles are involved in the conduction. For highly conductive composites, in which the filler volume fraction exceeds the critical percolation volume, the number of particles involved in the electrical conduction is maximum and the metal platelets form a closely packed conductive skeleton. Following Ruschau et al.,[58] for samples thick enough, i.e. much larger than the platelets dimensions, we can assume that each metal platelet and each chain contribute equally to the current conduction.

(iii) We assume that all the platelets have the same lateral dimensions. In our calculation to the average dimensions are used, as measured from SEM. From Eq. 1 we see that the platelets dimensions do not affect the intrinsic resistivity, which only depends on the filler fraction. The tunnelling and the constriction resistivity, on the other hand, depend linearly from the platelets thickness and are inversely proportional to the contact diameter/area (in turn related to the platelets lateral dimension). The spread in the platelets thickness (25%) does not affect significantly the theoretical predictions. A much larger distribution is observed in the lateral dimensions (1 µm to 15 µm). A rough estimate of the error made by neglecting the platelets size distribution is obtained by averaging the resistivity in Eq. 1 over the platelets size distribution observed by SEM. A discrepancy not larger than 30% is found, due to the fact that platelets larger the average contribute to decrease the sample resistivity and balance the effect of the smaller ones, which tend to increase the resistivity.

(iv) The tunnelling resistivity is assumed to be the same for any particles-pair and corresponding to a polymer thickness of 1nm. This is a critical parameter that only influences predictions in the tunnelling-conductivity picture.

Electrical conductivity in CAs added with nanocarbon fillers

Adding CNTs and graphene to the metal-filled adhesive results in a three components system. The carbon nanostructures are embedded in the polymer matrix and in contact with the metal platelets. The processes that lead to conductivity enhancement are currently under debate.[42] Indeed the nanostructures do interact with the metal platelets and the polymer matrix. The interaction depends on the nanofiller dimensions and volume concentration, as well as on the surface properties (e.g. presence of functional groups) and the processing conditions (temperature, viscosity).[57] Such

parameters determine the range and strength of interaction among the carbon nanoparticles, and their contact with the metal platelets. In a very simplified view of the system, at low volume concentration (i) the nanostructures can bridge metal platelets located far apart, adding new percolation paths among the metal platelets, thus increasing N_{paths}. At the same time, (ii) they can better link adjacent platelets, both decreasing the tunnel resistivity and increasing the diameter of the contact points, with the final result of a lower platelet-to-platelet constriction resistance. In presence of metal-decorated carbon nanostructures (iii) sintering between the nanometric metal particles and the micrometric metal platelets can increase the contact area, lowering the contact resistance. (iv) At concentrations overcoming the CNT/grephene-polymer percolation threshold (0.05% w/w according to Kirkpatrick's random resistors model,[57] ca. 0.1% v/v for graphene[21]) the carbon nanostructures can form additional "all-carbon" percolation paths allowing the electrons to flow from one electrode to the other by jumping, e.g., from CNT to CNT. These "all carbon" propagation mechanisms have shown a limited influence to the overall conductivity of the composites. Whereas DWNTs ropes have been synthetized with a resistivity that can go down to 100 – 200 μΩ cm after chemical tratment,[10] polymer composites filled with nanotubes typically feature conductivities that only exceptionally have reached 10^4 S/m, corresponding to a resistivity of 10^4 μΩ cm (see ref. [22] for a review). On the other hand, whereas graphene has been reported to have a conductivity up to 10^6 S/cm,[15] the typical resistivity of graphene-based composites is only ~ 10^5 – 10^6 Ω cm.[24,61] The reduction of the electrical resistivity in ECAs down to 10 – 100 μΩ cm[38] due to addition of a secondary filler based on nanostructured carbon is, indeed, a consequence of a synergic effect between the carbon and the metal filler, but it must be noted that the main conduction paths still occur through the metallic platelets. As shown in refs. [61,62], in fact, the resistivity of epoxies added with CNTs as a primary filler is orders of magnitude larger than the one reached after the addition of a metallic filler to the CNTs, although the presence of CNTs decreases the critical concentration at which the percolation among the metal particles does occur. This suggests that the carbon nanostructures somehow improve the contact among the metallic platelets.

Concerning our case, the addition of 1% wt. of DWNTs (equivalent to a volume concentration $f_{\mathrm{CNT}} = 2.2\%$) brings the effective resistivity down to $\rho_{\mathrm{eff}}^{\mathrm{cnt}} = 50 - 100$ μΩ cm. If we consider the nanotubes acting as an independent conductive network, not interacting with the primary silver filler, the best effective sample resistivity to be expected is $\rho_{\mathrm{eff}}^{\mathrm{CNT}} = \rho_{\mathrm{CNT}}/f_{\mathrm{CNT}} \sim 4 \times 10^3$ μΩ cm (see Note 2 in Supporting Information), i.e. 40 – 80 times higher than the measured one. In the same way, if we calculate the conductivity of the composite with the law of mixture

$$\sigma_{\mathrm{comp}} = f_{\mathrm{CNT}}\, \sigma_{\mathrm{CNT}} + f_{\mathrm{resin}}\, \sigma_{\mathrm{resin}} \tag{2}$$

where f_{resin} is the Ag-based resin volume fraction (97.8%), $\sigma_{\mathrm{resin}} \sim 3000$ S/cm is its conductivity, $\sigma_{\mathrm{CNT}} \sim 10^3 - 10^4$ S/cm the CNT conductivity (corresponding to minimum resistivity values measured in the literature), and $f_{\mathrm{CNT}} = 2.2\%$ we easily see that the expected contribution of the CNT network is negligible. This quantitatively proves that, at such low volume fractions, the nanotubes are by far less efficient than the silver platelets in driving electrons through the composite. Same discussion holds for GNPs, where an even better conductivity (minimum resistivity goes down to 30 μΩ cm) is observed at much lower concentrations.

Experiments tell us that the addition of pure solvent to the part A has detrimental effects on the electrical conductivity of the resin. The addition of CNTs and GNPs into the solvent, conversely, allows one to reduce the resistivity by a factor ten (30 – 50 μΩ cm) even at very low concentrations. This indicates that some synergic interaction among the metal platelets takes places, triggered by the presence of the carbon nanostructures. Furthermore, the observation of large conductivity improvements with pure carbon nanostructures, not decorated with metal NPs, proves that the sintering effect played by the metal NPs (iii) is not an important factor, at least for our systems. These results suggest that mechanisms (i), increase of the number of conduction paths, and (ii), improved contact among the platelets, are the only responsible for the conductivity improvement. As we have seen above, however, the increase of number of percolation paths due to the formation of an "all carbon" network has negligible effects, because of the small quantity of carbon nanostructures. At this stage our model can help to get insight on the role played by the carbon

nanoparticles in improving the contact among platelets. As seen in the previous section, the resistivity of the neat resin can be explained either assuming that conduction occurs via tunnelling among polymer-coated silver platelets through contact areas of few microns diameter [Figure 11(orange line)], or that current flows through contact points of average diameter ~10nm [Figure 11(blue line)]. On the other hand, resistivity values below 100 μΩ cm, as those obtained with the addition of carbon nanostructures to our resin, can only be justified in a physical picture in which electrons flow through nanometric contact points and the constriction resistance dominates the resistivity of the composite. According to our calculations [dashed box in Figure 11] resistivity values of 30 – 50 μΩ cm are possible for average contact point diameters ~ 100nm. The role of the carbon nanostructures is therefore to foster the electrical contact among the metallic platelets. One possible scenario for this to happen is that, when the polymer layer is locally dissolved by the solvent added to the part A of the resin, some contact among the metal platelets and the carbon nanostructures do establish. After curing, the original metal-polymer-metal interface, featuring high tunnelling resistance, is modified on the local scale into a metal-CNT/GNP-metal interface (as sketched in Figure 10g) characterized by average contact point diameter of ~100nm. In the same way, if we start with the assumption that the conductivity of the neat resin is already ruled by the constriction resistance, the effect of the nanostructures would be that of enhancing the average contact point diameter from 10 to 100nm thanks to the physical link with the metal platelets fostered by the action of the solvent. As suggested by Ruschau et al.[58] for metal platelets, a possible mechanism enabling such a link could be capillarity. When two particles are bridged by a liquid layer, the particles can be pushed together so to minimize the surface energy. During the curing phase, when temperatures are of the order of 100 – 150 °C, higher than the polymer Tg, CNTs/GNPs could be driven to bind to metal platelets by high capillary forces due to small liquid volumes and high curvature and surface energies.

Thermal conductivity increase in CAs and in CAs added with carbon nanostructures

Different numerical approaches have been proposed to describe the thermal conductivity of composites with misoriented fibers,[63] composites with coated reinforcement[64] and resins added with silver flakes.[58] Analytical models lead to formulas simpler to calculate. Among these the rule of mixture, the series model and the effective medium approximation (EMA) are the most widely used. [29,65,66] In the mixture model each phase is assumed to contribute independently and proportionally to its volume fraction, yielding a composite thermal conductivity

$$K_{\mathrm{comp}} = f_{\mathrm{filler}}\, K_{\mathrm{filler}} + f_{\mathrm{matrix}}\, K_{\mathrm{matrix}} \qquad (3)$$

where $f_{\mathrm{filler\ (matrix)}}$ and $K_{\mathrm{filler\ (matrix)}}$ are the filler (matrix) volume fraction and thermal conductivity. The rule of mixture implicitly assumes perfect contact among the filler particles, in a fully percolating network that maximizes the contribution of the conductive phases. The series model, conversely, assumes no direct contact between the filler particles. Conduction occurs through a filler-matrix-filler-matrix succession, yielding a composite conductivity

$$K_{\mathrm{comp}} = \frac{1}{f_{\mathrm{filler}}/\,K_{\mathrm{filler}} + f_{\mathrm{matrix}}/\,K_{\mathrm{matrix}}} \qquad (4)$$

The EMA model is based on the general Maxwell-Garnett effective medium theory that applies to transport problems in a medium in which the conductivity varies from point to point. This approach assumes that the conductive particles are isolated in the matrix and heath propagation occurs through the interface thermal resistance (Kapitza resistance). The interface resistance is consequence of the different phonon spectra of the materials phases and depends on the quality of the thermal contact at the interfaces. The large interface thermal resistance between matrix and filler is responsible of the low thermal conductivity of the composites. Nan et al.[66] have tailored the EMA approach to describe composites filled with particles of different orientation, size, shape and aspect ratios, a parameter known to strongly affect the conduction properties of the composites. The thermal conductivity in CNTs composites is obtained approximating the nanotubes as prolate spheroids, giving[67]

$$K_{\text{comp}} = \frac{3\ K_{\text{matrix}} + f_{\text{filler}}\ K_{\text{filler}}}{3 - 2f_{\text{filler}}} \tag{5}$$

GNPs, on the other hand, can be approximated as oblate spheroids, yielding the following expression for the thermal conductivity of the composites[16,68]

$$K_{\text{comp}} = \frac{3\ K_{\text{matrix}} + 2\ f_{\text{filler}}\ (K_{\text{filler}} - K_{\text{matrix}})}{(3 - f_{\text{filler}})\ K_{\text{filler}} + f_{\text{filler}}\ K_{\text{matrix}}} \tag{6}$$

The mixture model provides an upper bound to the thermal conductivity of the composite. The series model provides a lower bound to the conductivity of a two-components composite. Several "higher-order" models have been developed, fitting most of the experimental data (see ref. [29] for a review). We won't go into the details of these latter models.

From the thermal point of view, conductive adhesives behave in totally different way with respect to the electrical one. While the electrical conductivity of the silver filler is in more than 15 orders of magnitude larger than the resin ($\rho_{\text{resin}} > 10^{10}$ Ω cm),[7,22] such difference reduces to 3 – 4 orders of magnitude for the thermal conductivity ($K_{\text{T,resin}} \sim 10^{-1}$ W/m K).[30,] One immediate consequence is the absence of sharp percolation thresholds in the thermal conductivity curve, due to non-negligible residual heat conduction through the polymer matrix.[7,58] From the quantitative point of view, the thermal conductivity improvement in polymeric resins added with metallic fillers is typically limited to a factor 10 – 100, well below the improvements in the electrical conductivity (more than 15 orders of magnitude).

The addition of carbon nanostructures as a secondary filler in metal-added CAs is expected to strongly improve the thermal conductivity of the composites. The thermal conductivity of CNTs/GNPs is, in fact, 1.5 to 15 times larger than that of silver ($K_{\text{T, Ag}}$ = 430 W/m K against $K_{\text{T, CNT/GNP}}$ = 600 – 6000 W/m K). To our best knowledge no models describing the thermal properties of three components resins have been proposed so far. The physics of heat transport in the polymer-metal-nanocarbon composites is, indeed, complicated. Thermal conduction in nanotubes and graphene, as for the polymeric resin, is ruled by acoustic phonons, while in silver electrons drive the heat. [12] At the interfacial thermal barrier among the different materials thermal energy propagation

occurs via phonon-phonon scattering and phonon-electron scattering. The transmission of a phonon between the different phases depends on the existence of common vibration frequencies for the two phases and is supposed to occur only in the low frequency acoustic branches. In order to draw some conclusion on the role played by the carbon nanostructures, we will apply models developed for two-components composites and critically discuss to what extent the addition of small fractions of CNTs and GNPs can provide alternative heath conduction pathways with respect to the metal platelets. To this aim we will consider our starting resin as a (conductive) matrix featuring thermal conductivity $K_{T,resin}$ = 2.6 W/mK (the value measured on the starting resin) filled with carbon nanotubes ($K_{T, CNT}$ = 750 – 7000 W/m K) [12,13] or graphene nanoplatelets ($K_{T, GNP}$ = 650 – 5000 W/m K) [12,16,17] at different concentrations. Figure 12 compares the thermal conductivity measured on the CNTs- (a) and GNPs- (b) nanocomposites with the predictions from the three major analytical models: mixture (blue lines), series (green lines) and Nan's model (red lines) for CNTs (Eq. 5) and graphene (Eq. 6).

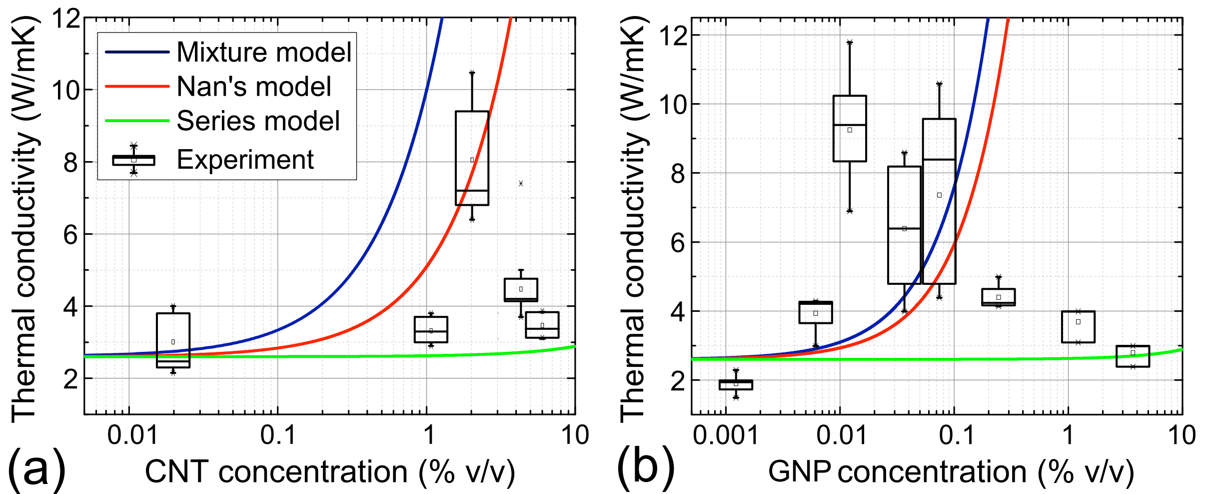

Figure 12: Plots of the thermal conductivity measured on nanocomposites prepared with the addition of CNTs- (a) and GNPs- (b) at different volume concentrations compared with the theoretical predictions based on the series (green lines), mixture (blue lines) and Nan's models adapted for graphene and CNTs (red lines). Thermal conductivity of CNTs and GNPs is assumed to be, respectively, $K_{T, CNT}$ = 750 W/m K and $K_{T, GNP}$ = 5000 W/m K. The volume concentrations are calculated assuming mass densities of 1.2 g/cm^3 and 2.2 g/cm^3 for CNTs and GNPs, respectively.

For the CNTs composites the maximum thermal conductivity measured at 2.2% volume fraction is compatible with the value predicted by Nan's model, if we assume a thermal conductivity of CNTs $K_{T,\,CNT}$ = 750 W/m K, i.e. the minimum value found in the literature. This suggests that, differently from the electrical resistivity, at a volume concentration of 2.2 %v/v a network of CNTs could in principle justify the thermal conductivity increase observed. For GNPs the situation is different. A thermal conductivity higher than 8 W/mK is observed at volume concentrations ranging from 0.012 to 0.07 %v/v. For such low concentrations, neither Nan's model nor the mixture model can predict such a large conductivity increase, even assuming the maximum thermal conductivity found in literature for the GNPs, $K_{T,\,GNP}$ = 5000 W/m K. Such a result suggests that, as such low GNPs concentrations, heat is driven by the metallic network, and as for the electrons. The role of GNPs is to foster the thermal contact among the silver particles, partially replacing the polymer at the metal-metal interface. The increase of the thermal conductivity is therefore a result of a smaller thermal interface resistance due to a better contact among the filler particles.

Goyal et al.[43] achieved 10 W/mK thermal conductivity with few layers graphene at ~ 3 wt%. Here we find that it is possible to reach thermal conductivities up to ~ 12 W/mK with weight fractions of GNP as small as 0.01 %w/w. We attribute such an improvement to the use of IPA as a common solvent capable to dissolve the resin and foster the metal-nanocarbon-metal contact.

Optimal conductivity CAs added with nanocarbon fillers

In ECAs an increased concentration of carbon nanostructures does not necessarily imply an improvement of the electric transport properties. Wu et al.[69] and Oh et al. [39,40], working on nanocomposites filled with Ag-decorated MWNTs, already noted the presence of an optimal filler concentration beyond which the electrical conductivity soon returned back to the one of the untreated resin. Our results are in agreement, also quantitative, with Oh et al., suggesting that optimal electrical conductivity in ECAs is obtained by adding 1 to 3% w/w of CNTs. In our

experiments we have found this effect also with GNPs, at much smaller thresholds (~ 0.2% w/w). In addition, an even more critical dependence is observed for the thermal conductivity. The conductivity worsening observed beyond the optimal concentration of carbon nanostructures, when used as secondary filler, can be understood considering that in the nanostructured composite the shrinking due to the formation of the cross-links is associated with a dragging of the carbon nanostructures dispersed in the epoxy matrix. Enhanced conductivity is therefore expected only if the nanostructured filler is capable to foster the contact with the silver platelets, i.e. to increase the effective contact area. As discussed above, this can occur either through an intercalation of the carbon nanostructures at the interface between metal platelets, or through a local replacement of the residual polymeric layer by the CNTs/GNPs. The steric hindrance of clustered CNTs, due to phase segregation or bad dispersion, as well as the occurrence of large graphitic pieces, will worsen the networking with the silver micro-platelets and, consequently, prevent the achievement of the optimal conditions that permit the enhancement of the conductivity. As a result the conductivity of the resin will turn back its pristine values, or even worsen (whenever the carbon aggregates start to hamper the networking of the primary filler). The SEM image in Figure S6 (Supporting Information) supports this scenario. Here we show a nanocomposite prepared with 4% of DWNTs, in which we observe microscopic aggregates of nanotubes embedded in the epoxy resin that tend to separate the silver particles. A similar morphology is observed at high GNPs loadings (not shown). The fact that both the electrical and thermal conductivity show similar trends as a function of the concentration suggests that the mechanisms underlying the conductivity improvement are basically the same. The higher sensitivity of the thermal conductivity on the CNTs concentration suggests that the achievement of a conditions featuring optimal thermal propagation is more critical to be obtained.

CONCLUSIONS

In summary, we have shown that double-wall carbon nanotubes and graphene nanoplatelets incorporated into silver-added commercial resins yield conductive adhesives featuring, simultaneously, enhanced thermal (up to +470%) and electrical conductivity (up to +1100%). An efficient dispersion of the carbon nanostructures into the epoxy resin is achieved using isopropyl alcohol as a common solvent, capable to simultaneously debundle the CNTs, exfoliate the GNPs and dissolve the resin. Conductivity enhancements are observed at very low loadings, namely 1% w/w for CNTs and 0.01% w/w for GNPs, without the need of additional decoration steps with metal nanoparticles. GNPs yield better performances than DWNTs, improving the thermal conductivity of the resin from 2.6 to 11.8 W/mK and reducing the resistivity from 350 to 33 μΩ cm, at much smaller loadings. A comparison with theoretical models suggests that, at such low concentrations, the role of the carbon nanostructures is to foster the electrical and thermal contact among the platelets, thus reducing the interface resistance. The reduced quantity of carbon nanostructures permits to keep almost unchanged the thermodynamic and mechanical properties of the resulting nanocomposites. In particular, we show that the bonding properties do satisfy the MIL-STD-883 standard, even after repeated thermal cycling. The same loading procedure has been successfully applied to disperse CNTs and GNPs into a more viscous, higher conductivity adhesive, resulting in a doubling of the thermal conductivity and a fourfold increase of the electrical conductivity. We finally employ the nanostructured resins to bond GaN transistor into RF power amplifier circuits, finding a remarkable decrease of the MMICs operation temperature (30°C reduction of the peak temperature, 10 °C of the average temperature). Major advantages of our technique are the use of readily available graphite, simplicity of the process, low cost and scalability of production. The proposed route could be a fast vehicle for the incorporation of carbon nanostructures in a wide range of industrial applications (aerospace, automotive, etc.) whenever high power dissipation is a concern. Our results are among the technological development steps foreseen by the graphene roadmap.[70]

Supporting information

Additional information is provided showing SEM images of the neat resin, a comparative plot of the conductivity properties of nanocomposites filled with HOPG, DWNT and GNPs, a plot with die shear strength criteria according to the MIL-STD-883, the schematic of the metal filler used to develop the theoretical model, the plot of the tunneling resistivity Vs polymer film thickness, a SEM image of the resin added with 4% w/w DWNTs. Two notes are also added with the detail of the ECAs electrical conductivity model and the estimate of the pure CNTs network resistivity.

Acknowledgments

This work has been funded by MIUR under the project PON01_01322 PANREX “Packaging basato su nanomateriali per Ricevitori ed Exciter compatti per Applicazioni Radar con Antenna a scansione elettronica del fascio,” that is greatly acknowledged.

REFERENCES

(1) Li, Y.; Wong, C., Recent Advances of Conductive Adhesives as a Lead-Free Alternative in Electronic Packaging: Materials, Processing, Reliability and Applications. *Mater. Sci. Eng. R* **2006,** *51*, 1-35.

(2) Gwinn, J. P.; Webb, R., Performance and Testing of Thermal Interface Materials. *Microelectron. J.* **2003,** *34*, 215-222.

(3) Sepulveda, J. L.; Vandermark, L. J. In *RF and Microwave Microelectronics Packaging*, 1st ed; Kuang, K.; Kim, F.; Cahill, S. S., Eds.; Springer-Verlag: Berlin Heidelberg, 2010; Chapter 10, pp 207-232.

(4) See, for example, Epotek technologies (www.epotek.com) and DIEMAT/NAMICS products, (www.diemat.com)

(5) Lovinger, A. J., Development of Electrical Conduction in Silver-Filled Epoxy Adhesives. *J. Adhes.* **1979,** *10,* 1-15.

(6) Lu, D.; Tong, Q. K.; Wong, C. P. In *Conductivity Mechanisms of Isotropic Conductive Adhesives (Icas)*, Advanced Packaging Materials: Processes, Properties and Interfaces, 1999. Proceedings. International Symposium on, IEEE: **1999**; pp 2-10.

(7) Mamunya, Y. P.; Davydenko, V.; Pissis, P.; Lebedev, E., Electrical and Thermal Conductivity of Polymers Filled with Metal Powders. *Eur. Polym. J.* **2002,** *38*, 1887-1897.

(8) Dai, H.; Wong, E. W.; Lieber, C. M., Probing Electrical Transport in Nanomaterials: Conductivity of Individual Carbon Nanotubes. *Science* **1996,** *272*, 523-526.

(9) Charlier, J.-C.; Blase, X.; Roche, S., Electronic and Transport Properties of Nanotubes. *Rev. Mod. Phys.* **2007,** *79*, 677-732.

(10) Zhao, Y.; Wei, J.; Vajtai, R.; Ajayan, P. M.; Barrera, E. V., Iodine Doped Carbon Nanotube Cables Exceeding Specific Electrical Conductivity of Metals. *Sci. Rep.* **2011,** *1*, 1.

(11) Wei, J.; Zhu, H.; Jiang, B.; Ci, L.; Wu, D., Electronic Properties of Double-Walled Carbon Nanotube Films. *Carbon* **2003,** *41*, 2495-2500.

(12) Balandin, A. A., Thermal Properties of Graphene and Nanostructured Carbon Materials. *Nat. Mater.* **2011,** *10*, 569-581.

(13) Choi, T.-Y.; Poulikakos, D.; Tharian, J.; Sennhauser, U., Measurement of the Thermal Conductivity of Individual Carbon Nanotubes by the Four-Point Three-Ω Method. *Nano Lett.* **2006,** *6*, 1589-1593.

(14) Bolotin, K. I.; Sikes, K.; Jiang, Z.; Klima, M.; Fudenberg, G.; Hone, J.; Kim, P.; Stormer, H., Ultrahigh Electron Mobility in Suspended Graphene. *Solid State Commun.* **2008,** *146*, 351-355.

(15) Zhang, L. L.; Zhou, R.; Zhao, X., Graphene-Based Materials as Supercapacitor Electrodes. *J. Mater. Chem.* **2010,** *20*, 5983-5992.

(16) Balandin, A. A.; Ghosh, S.; Bao, W.; Calizo, I.; Teweldebrhan, D.; Miao, F.; Lau, C. N., Superior Thermal Conductivity of Single-Layer Graphene. *Nano Lett.* **2008,** *8*, 902-907.

(17) Ghosh, S.; Bao, W.; Nika, D. L.; Subrina, S.; Pokatilov, E. P.; Lau, C. N.; Balandin, A. A., Dimensional Crossover of Thermal Transport in Few-Layer Graphene. *Nat. Mater.* **2010,** *9*, 555-558.

(18) Kaur, S.; Raravikar, N.; Helms, B. A.; Prasher, R.; Ogletree, D. F., Enhanced Thermal Transport at Covalently Functionalized Carbon Nanotube Array Interfaces. *Nat. Commun.* **2014,** *5*, 3082.

(19) Yan, Z.; Liu, G.; Khan, J. M.; Balandin, A. A., Graphene Quilts for Thermal Management of High-Power Gan Transistors. *Nat. Commun.* **2012,** *3*, 827.

(20) Moniruzzaman, M.; Winey, K. I., Polymer Nanocomposites Containing Carbon Nanotubes. *Macromolecules* **2006,** *39*, 5194-5205.

(21) Stankovich, S.; Dikin, D. A.; Dommett, G. H.; Kohlhaas, K. M.; Zimney, E. J.; Stach, E. A.; Piner, R. D.; Nguyen, S. T.; Ruoff, R. S., Graphene-Based Composite Materials. *Nature* **2006,** *442*, 282-286.

(22) Bauhofer, W.; Kovacs, J. Z., A Review and Analysis of Electrical Percolation in Carbon Nanotube Polymer Composites. *Compos. Sci. Technol.* **2009,** *69*, 1486-1498.

(23) Liu, Y.; Kumar, S., Polymer/Carbon Nanotube Nano Composite Fibers–a Review. *ACS Appl. Mater. Interfaces* **2014,** *6*, 6069-6087.

(24) Kuilla, T.; Bhadra, S.; Yao, D.; Kim, N. H.; Bose, S.; Lee, J. H., Recent Advances in Graphene Based Polymer Composites. *Prog. Polym. Sci.* **2010,** *35*, 1350-1375.

(25) Ramasubramaniam, R.; Chen, J.; Liu, H., Homogeneous Carbon Nanotube/Polymer Composites for Electrical Applications. *Appl. Phys. Lett.* **2003,** *83*, 2928-2930.

(26) De Volder, M. F.; Tawfick, S. H.; Baughman, R. H.; Hart, A. J., Carbon Nanotubes: Present and Future Commercial Applications. *Science* **2013,** *339*, 535-539.

(27) Huxtable, S. T.; Cahill, D. G.; Shenogin, S.; Xue, L.; Ozisik, R.; Barone, P.; Usrey, M.; Strano, M. S.; Siddons, G.; Shim, M., Interfacial Heat Flow in Carbon Nanotube Suspensions. *Nat. Mater.* **2003,** *2*, 731-734.

(28) Jones, W. E.; Chiguma, J.; Johnson, E.; Pachamuthu, A.; Santos, D., Electrically and Thermally Conducting Nanocomposites for Electronic Applications. *Materials* **2010,** *3*, 1478-1496.

(29) Han, Z.; Fina, A., Thermal Conductivity of Carbon Nanotubes and Their Polymer Nanocomposites: A Review. *Prog. Polym. Sci.* **2011,** *36*, 914-944.

(30) Teng, C.-C.; Ma, C.-C. M.; Lu, C.-H.; Yang, S.-Y.; Lee, S.-H.; Hsiao, M.-C.; Yen, M.-Y.; Chiou, K.-C.; Lee, T.-M., Thermal Conductivity and Structure of Non-Covalent Functionalized Graphene/Epoxy Composites. *Carbon* **2011,** *49*, 5107-5116.

(31) Li, J.; Ma, P. C.; Chow, W. S.; To, C. K.; Tang, B. Z.; Kim, J. K., Correlations between Percolation Threshold, Dispersion State, and Aspect Ratio of Carbon Nanotubes. *Adv. Funct. Mater.* **2007,** *17*, 3207-3215.

(32) Moon, J.; Weaver, K.; Feng, B.; Chae, H. G.; Kumar, S.; Baek, J.-B.; Peterson, G., Note: Thermal Conductivity Measurement of Individual Poly (Ether Ketone)/Carbon Nanotube Fibers Using a Steady-State Dc Thermal Bridge Method. *Rev. Sci. Instrum.* **2012,** *83*, 016103.

(33) Yu, A.; Ramesh, P.; Itkis, M. E.; Bekyarova, E.; Haddon, R. C., Graphite Nanoplatelet-Epoxy Composite Thermal Interface Materials. *J. Phys. Chem. C* **2007,** *111*, 7565-7569.

(34) Li, Q.; Guo, Y.; Li, W.; Qiu, S.; Zhu, C.; Wei, X.; Chen, M.; Liu, C.; Liao, S.; Gong, Y., Ultrahigh Thermal Conductivity of Assembled Aligned Multilayer Graphene/Epoxy Composite. *Chem. Mater.* **2014,** *26*, 4459-4465.

(35) Shtein, M.; Nadiv, R.; Buzaglo, M.; Regev, O., Graphene-Based Hybrid Composites for Efficient Thermal Management of Electronic Devices. *ACS Appl. Mater. Interfaces* **2015,** *7*, 23725-23730.

(36) Shahil, K. M.; Balandin, A. A., Graphene–Multilayer Graphene Nanocomposites as Highly Efficient Thermal Interface Materials. *Nano Lett.* **2012,** *12*, 861-867.

(37) Haddon, R. C.; Itkis, M. E.; Ramesh, P.; Yu, A.; Bekyarova, E.; Worseley, K. Graphite nanoplatelets for thermal and electrical applications. U.S. Patent Application US20140014871 A1, July, 11, 2013.

(38) Amoli, B. M.; Hu, A.; Zhou, N. Y.; Zhao, B., Recent Progresses on Hybrid Micro–Nano Filler Systems for Electrically Conductive Adhesives (Ecas) Applications. *J. Mater. Sci-Mater. El.* **2015,** *26*, 4730-4745.

(39) Oh, Y.; Suh, D.; Kim, Y.; Lee, E.; Mok, J. S.; Choi, J.; Baik, S., Silver-Plated Carbon Nanotubes for Silver/Conducting Polymer Composites. *Nanotechnology* **2008,** *19*, 495602.

(40) Oh, Y.; Chun, K.-Y.; Lee, E.; Kim, Y.-J.; Baik, S., Functionalized Nano-Silver Particles Assembled on One-Dimensional Nanotube Scaffolds for Ultra-Highly Conductive Silver/Polymer Composites. *J. Mater. Chem.* **2010,** *20*, 3579-3582.

(41) Liu, K.; Liu, L.; Luo, Y.; Jia, D., One-Step Synthesis of Metal Nanoparticle Decorated Graphene by Liquid Phase Exfoliation. *J. Mater. Chem.* **2012,** *22*, 20342-20352.

(42) Amoli, B. M.; Trinidad, J.; Hu, A.; Zhou, Y. N.; Zhao, B., Highly Electrically Conductive Adhesives Using Silver Nanoparticle (Ag Np)-Decorated Graphene: The Effect of Nps Sintering on the Electrical Conductivity Improvement. *J. Mater. Sci-Mater. El.* **2015,** *26*, 590-600.

(43) Goyal, V.; Balandin, A. A., Thermal Properties of the Hybrid Graphene-Metal Nano-Micro-Composites: Applications in Thermal Interface Materials. *Appl. Phys. Lett.* **2012,** *100*, 073113.

(44) Bonaccorso, F.; Hasan, T.; Tan, P.; Sciascia, C.; Privitera, G.; Di Marco, G.; Gucciardi, P.; Ferrari, A., Density Gradient Ultracentrifugation of Nanotubes: Interplay of Bundling and Surfactants Encapsulation. *J. Phys. Chem. C* **2010,** *114*, 17267-17285.

(45) Xie, X.-L.; Mai, Y.-W.; Zhou, X.-P., Dispersion and Alignment of Carbon Nanotubes in Polymer Matrix: A Review. *Mater. Sci. Eng. R* **2005,** *49*, 89-112.

(46) Hernandez, Y.; Nicolosi, V.; Lotya, M.; Blighe, F. M.; Sun, Z.; De, S.; McGovern, I.; Holland, B.; Byrne, M.; Gun'Ko, Y. K., High-Yield Production of Graphene by Liquid-Phase Exfoliation of Graphite. *Nat. Nanotechnol.* **2008,** *3*, 563-568.

(47) O'Neill, A.; Khan, U.; Nirmalraj, P. N.; Boland, J.; Coleman, J. N., Graphene Dispersion and Exfoliation in Low Boiling Point Solvents. *J. Phys. Chem. C* **2011,** *115*, 5422-5428.

(48) Rafiee, M. A.; Rafiee, J.; Wang, Z.; Song, H.; Yu, Z.-Z.; Koratkar, N., Enhanced Mechanical Properties of Nanocomposites at Low Graphene Content. *ACS Nano* **2009,** *3*, 3884-3890.

49 Kravets, V.; Grigorenko, A.; Nair, R.; Blake, P.; Anissimova, S.; Novoselov, K.; Geim, A., Spectroscopic Ellipsometry of Graphene and an Exciton-Shifted Van Hove Peak in Absorption. *Phys. Rev. B* **2010,** *81*, 155413.

(50) Khan, U.; O'Neill, A.; Lotya, M.; De, S.; Coleman, J. N., High‐Concentration Solvent Exfoliation of Graphene. *Small* **2010,** *6*, 864-871.

(51) Ferrari, A.; Meyer, J.; Scardaci, V.; Casiraghi, C.; Lazzeri, M.; Mauri, F.; Piscanec, S.; Jiang, D.; Novoselov, K.; Roth, S., Raman Spectrum of Graphene and Graphene Layers. *Phys. Rev. Lett.* **2006,** *97*, 187401.

(52) Maragó, O. M.; Bonaccorso, F.; Saija, R.; Privitera, G.; Gucciardi, P. G.; Iatì, M. A.; Calogero, G.; Jones, P. H.; Borghese, F.; Denti, P., Brownian Motion of Graphene. *ACS Nano* **2010,** *4*, 7515-7523.

(53) Haar, S.; El Gemayel, M.; Shin, Y. Y.; Melinte, G.; Squillaci, M. A.; Ersen, O.; Casiraghi, C.; Ciesielski, A.; Samori, P., Enhancing the Liquid-Phase Exfoliation of Graphene in Organic Solvents Upon Addition of N-Octylbenzene. *Sci. Rep.* **2015,** *5*, 16684.

(54) Prolongo, M. G.; Salom, C.; Arribas, C.; Sanchez-Cabezudo, M.; Masegosa, R. M.; Prolongo, S. G., Influence of Graphene Nanoplatelets on Curing and Mechanical Properties of Graphene/Epoxy Nanocomposites. *J. Therm. Anal. Calorim.* **2016,** *125*, 629-636.

55 Song, Y. S.; Youn, J. R., Influence of Dispersion States of Carbon Nanotubes on Physical Properties of Epoxy Nanocomposites. *Carbon* **2005,** *43*, 1378-1385.

(56) Liao, Y.-H.; Marietta-Tondin, O.; Liang, Z.; Zhang, C.; Wang, B., Investigation of the Dispersion Process of Swnts/Sc-15 Epoxy Resin Nanocomposites. *Mater. Sci. Eng., A* **2004,** *385*, 175-181.

(57) Mutiso, R. M.; Winey, K. I., Electrical Properties of Polymer Nanocomposites Containing Rod-Like Nanofillers. *Prog. Polym. Sci.* **2015,** *40*, 63-84.

58 Ruschau, G.; Yoshikawa, S.; Newnham, R., Resistivities of Conductive Composites. *J. Appl. Phys.* **1992,** *72*, 953-959.

(59) Kim, W.; Taya, M.; Nguyen, M., Electrical and Thermal Conductivities of a Silver Flake/Thermosetting Polymer Matrix Composite. *Mech. Mater.* **2009,** *41*, 1116-1124.

(60) Mamunya, Y.; Boudenne, A.; Lebovka, N.; Ibos, L.; Candau, Y.; Lisunova, M., Electrical and Thermophysical Behaviour of Pvc-Mwcnt Nanocomposites. *Compos. Sci. Technol.* **2008,** *68*, 1981-1988.

(61) Pu, N.-W.; Peng, Y.-Y.; Wang, P.-C.; Chen, C.-Y.; Shi, J.-N.; Liu, Y.-M.; Ger, M.-D.; Chang, C.-L., Application of Nitrogen-Doped Graphene Nanosheets in Electrically Conductive Adhesives. *Carbon* **2014,** *67*, 449-456.

(62) Marcq, F.; Demont, P.; Monfraix, P.; Peigney, A.; Laurent, C.; Falat, T.; Courtade, F.; Jamin, T., Carbon Nanotubes and Silver Flakes Filled Epoxy Resin for New Hybrid Conductive Adhesives. *Microelectron. Reliab.* **2011,** *51*, 1230-1234.

(63) Hatta, H.; Taya, M., Effective Thermal Conductivity of a Misoriented Short Fiber Composite. *J. Appl. Phys.* **1985,** *58*, 2478-2486.

(64) Dunn, M. L.; Taya, M., The Effective Thermal Conductivity of Composites with Coated Reinforcement and the Application to Imperfect Interfaces. *J. Appl. Phys.* **1993,** *73*, 1711-1722.

(65) Hasselman, D.; Johnson, L. F., Effective Thermal Conductivity of Composites with Interfacial Thermal Barrier Resistance. *J. Compos. Mater.* **1987,** *21*, 508-515.

(66) Nan, C.-W.; Birringer, R.; Clarke, D. R.; Gleiter, H., Effective Thermal Conductivity of Particulate Composites with Interfacial Thermal Resistance. *J. Appl. Phys.* **1997,** *81*, 6692-6699.

(67) Nan, C.-W.; Shi, Z.; Lin, Y., A Simple Model for Thermal Conductivity of Carbon Nanotube-Based Composites. *Chem. Phys. Lett.* **2003,** *375*, 666-669.

(68) Xie, S.; Liu, Y.; Li, J., Comparison of the Effective Conductivity between Composites Reinforced by Graphene Nanosheets and Carbon Nanotubes. *Appl. Phys. Lett.* **2008,** *92*, 243121.

(69) Wu, H.; Wu, X.; Ge, M.; Zhang, G.; Wang, Y.; Jiang, J., Properties Investigation on Isotropical Conductive Adhesives Filled with Silver Coated Carbon Nanotubes. *Compos. Sci. Technol.* **2007,** *67*, 1182-1186.

(70) Ferrari, A. C.; Bonaccorso, F.; Fal'ko, V.; Novoselov, K. S.; Roche, S.; Bøggild, P.; Borini, S.; Koppens, F. H. L.; Palermo, V.; Pugno, N.; Garrido, J. A.; Sordan, R.; Bianco, A.; Ballerini, L.; Prato, M.; Lidorikis, E.; Kivioja, J.; Marinelli, C.; Ryhänen, T.; Morpurgo, A.; Coleman, J. N.; Nicolosi, V.; Colombo, L.; Fert, A.; Garcia-Hernandez, M.; Bachtold, A.; Schneider, G. F.; Guinea, F.; Dekker, C.; Barbone, M.; Sun, Z.; Galiotis, C.; Grigorenko, A. N.; Konstantatos, G.; Kis, A.; Katsnelson, M.; Vandersypen, L.; Loiseau, A.; Morandi, V.; Neumaier, D.; Treossi, E.; Pellegrini, V.; Polini, M.; Tredicucci, A.; Williams, G. M.; Hong, B. H.; Ahn, J. H.; Kim, J. M.; Zirath, H.; Van Wees, B. J.; Van der Zant, H.; Occhipinti, L.; Di Matteo, A.; Kinloch, A.; Seyller, T.; Quesnel, E.; Feng, X.; Teo, K.; Rupesinghe, N.; Hakonen, P.; Neil, S. R. T.; Tannock, Q.; Löfwander, T.; Kinaret, J. Science and Technology Roadmap for Graphene, Related Two-Dimensional Crystals, and Hybrid Systems. *Nanoscale* **2015,** *7*, 4598-4810.

Table of Contents